Mesoscale Circulation Growth under Conditions of Weak Inertial Instability

DAVID O. BLANCHARD*

NOAA/National Severe Storms Laboratory, Boulder, Colorado

WILLIAM R. COTTON

Department of Atmospheric Science, Colorado State University, Fort Collins, Colorado

JOHN M. BROWN

NOAA/Forecast Systems Laboratory, Boulder, Colorado

(Manuscript received 9 April 1996, in final form 29 April 1997)

ABSTRACT

The hypothesis that inertial instability plays a role in the upscale development of mesoscale convective systems (MCSs) is explored by sampling environments that supported the growth of MCSs in the Preliminary Regional Experiment for STORM (Stormscale Operational and Research Meteorology) (PRE-STORM) network with high quality special soundings. Secondary circulations that occurred in the presence of inertial instabilities were analyzed and documented using rawinsonde data with high spatial and temporal resolution from the PRE-STORM field program. Additional examples of MCS environments were examined using data from the Mesoscale Analysis and Prediction System. Results show strong divergence and cross-stream accelerations occurred at upper-tropospheric levels where inertial instabilities were present. These accelerations were not uniform over the domain but were focused in the regions of instability. Also, the analyses of these data showed that regions of inertial instability may be more commonplace than is typically assumed.

The Regional Atmospheric Modeling System was used to increase the understanding of the basic processes and secondary circulations that enhance MCS growth in inertially unstable environments. Model results indicate that the strength of the divergent outflow was strongly linked to the degree of inertial stability in the local environment. The results also showed a strong dependence on the magnitude of the Coriolis parameter. Finally, experiments using varying degrees of vertical stability indicated that there was also significant sensitivity to this parameter.

1. Introduction

The development of nocturnal mesoscale convective complexes (MCCs), described by Maddox (1980), and of the more general mesoscale convective systems (MCSs) has been shown to be a function of large-scale synoptic patterns; terrain-induced features, such as elevated heat sources; and localized mesoscale forcing (Maddox 1980; Cotton et al. 1983; Wetzel et al. 1983; Tripoli and Cotton 1989a). Using objective analysis and compositing techniques for 10 MCCs, Maddox (1983) identified several distinctive features at the surface and in the lower, middle, and upper troposphere during the formation, mature, and dissipation stages of MCCs. Cotton et al. (1989), using compositing techniques that permit greater temporal resolution, examined 134 MCC events and concluded that ''a mature MCC is an inertially stable form of an MCS that is nearly geostrophically balanced and whose horizontal scale is comparable to or greater than the (modified) Rossby radius of deformation, λ_R.'' The significance of λ_R is that it crudely identifies the scale at which rotational influences or the inertial stability of a system become important.

Nachamkin et al. (1994) examined data from the Preliminary Regional Experiment for Stormscale Operational and Research Meteorology (PRE-STORM; Cunning 1986) to describe the upscale evolution of an MCC. They noted that mesoscale organization occurred shortly after the upper-level cloud shield reached MCC proportions (i.e., scales comparable to λ_R) and the convective organization manifested itself as a rapid, almost discrete transition. They noted that their result agrees with the assertion made by McAnelly and Cotton (1992) that the upscale transition from separate convective clusters to a coherent MCC may occur early in the MCC

* Additional affiliation: Cooperative Institute for Mesoscale Meteorological Studies, University of Oklahoma, Norman, Oklahoma.

Corresponding author address: Dr. David O. Blanchard, NOAA/NSSL, 325 Broadway, Boulder, CO 80303.

life cycle and more abruptly than inferred from previous MCC life cycle research.

Tripoli and Cotton (1989a), using the Regional Atmospheric Modeling System (RAMS), investigated the genesis of an MCS that had its origins in the Colorado mountains. They were able to simulate both the mountain-generated solenoidal circulation and the solenoidal circulation that is located over the High Plains. Their results indicated that both features were important in the genesis of the MCS. The simulation, however, was restricted to two dimensions and could not accurately model the low-level jet, a feature of importance for MCS intensification. Nonetheless, they were able to simulate the upscale growth of convection from the meso-γ-scale to the larger meso-β-scale because of the growth of a deep meso-α-scale circulation. This result suggests the importance of the secondary circulations generated by the mesoscale convection.

Substantial effort has been made over many years to address the issues of convective evolution from the meso-γ scale to the meso-β and meso-α scales associated with MCCs and MCSs. Here, we address issues of scale interaction between the meso-β-scale convective processes and the mesoscale-α-scale environment. In section 2 we present a conceptual model and hypothesis in which upper-tropospheric inertial instability can enhance the upscale growth of meso-β-scale convective elements into a meso-α-scale convective system. Section 3 presents two example case studies and composite cases for 1990–93. Section 4 discusses the design of our numerical experiments, and section 5 reports on the results of these experiments. Section 6 presents a summary and conclusions, and section 7 suggests approaches to future research.

2. Conceptual model

A large part of the work on MCC/MCS development and evolution has concentrated on systems that can attribute a significant portion of the mesoscale organizing mechanisms to the presence of surface boundaries driven and maintained, in part, by synoptic-scale baroclinic waves traversing the region. Because of the frontogenetical nature of these waves, linear patterns of upward motion can be produced on the synoptic scale, resulting in similarly shaped regions of strong conditional or convective instability that is released by lifting associated with the passage of the surface boundary.

In contrast to the convective systems that often develop in an environment with strong embedded short waves and cyclonic vorticity, many MCCs and MCSs have been observed to form in environments where the isentropic absolute vorticity may have values that approach zero or are negative, resulting in regions with weak inertial stability or inertial instability. Further, if certain vertical stability criteria are also met, then symmetric instability may also be present. Symmetric instability, a fundamental instability in a rotating fluid, is

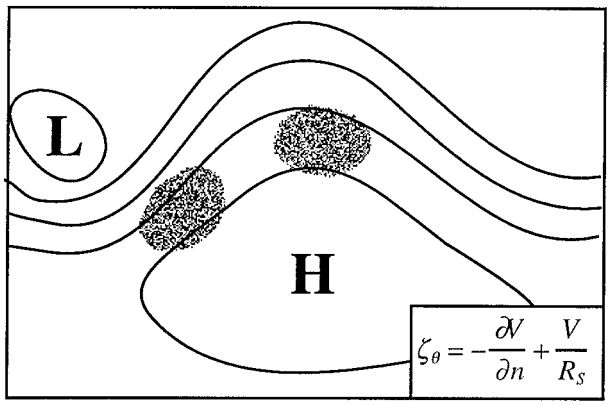

FIG. 1. Two typical regions in which mesoscale convective systems (MCSs; darkened regions) occur. Contours are representative of the Montgomery streamfunction (height) on isentropic (pressure) surfaces. Lows and highs marked by L and H, respectively. The equation for isentropic relative vorticity ζ_θ is given in natural coordinates. The first term on the right-hand side is the shear term and the second is the curvature term, where V is the wind speed, n is a distance oriented normal to the streamline, and R_s is the radius of curvature of the streamlines.

a combined buoyant-inertial instability that can be viewed as inertial instability on a buoyancy surface or buoyant instability on a surface of constant angular momentum (Xu 1986). It has been demonstrated that, for a given amount of convective available potential energy (CAPE), deep convective circulations can be modified and enhanced as the symmetric stability is reduced (Eliassen 1951; Emanuel 1982, 1983; Xu 1986).

Consequently, there has been speculation that the mesoscale evolution and organization of these MCCs and MCSs may be related to the existence of an environment in which the inertial stability is weak (Emanuel 1979, 1982; Jascourt et al. 1988; Seman 1990). Two typical regions in which inertial stability is weak or is unstable are 1) just equatorward of a westerly wind maximum where the anticyclonic shear is large, and 2) in subsynoptic-scale ridges where the anticyclonic curvature is large. Figure 1 is a schematic representation of both types of environments. The definition of isentropic relative vorticity ζ_θ is given in natural coordinates in the lower-right corner of the figure. The first term on the right-hand side is the shear term, which is large and negative equatorward of regions where jet streaks are present; the second term on the right is the curvature term, which is large and negative in ridges. Observations (Maddox 1983; Kane et al. 1987; Cotton et al. 1989; Blanchard 1990) indicate that these are preferred regions for the upscale development of convection into MCSs.

It has been shown (Eliassen 1951; Bennetts and Hoskins 1979; Emanuel 1979) that in an environment where the atmosphere is stable to vertical (buoyancy) and horizontal (inertial) displacements, displacement along certain slantwise paths may still be unstable if both rotation and static stability are considered together. Although

Eliassen (1951) applied this concept to the baroclinic circumpolar vortex, it can also be applied locally to jet streaks defined as meso-α-scale regions of enhanced upper flow embedded within the jet stream. If the flow in such a jet streak exhibits approximate geostrophic-thermal wind balance, then the geostrophic momentum M is approximately conserved in the absence of frictional and diabatic effects. A dry atmosphere is said to be symmetrically unstable if upward (downward) displacement along a surface of constant M results in a parcel's becoming warmer (cooler) than its environment. If a parcel of air at or near saturation is lifted along a surface of constant M and becomes warmer than its environment solely because of the release of latent heat, then the atmosphere is said to be in a state of conditional symmetric instability (CSI). A conditionally or convectively stable atmosphere may still be conditionally symmetrically unstable, allowing ''slantwise'' convection to take place.

In certain mesoscale environments, particularly in the springtime when large CAPE and a strong jet streak often coexist, the atmosphere may be both convectively and symmetrically unstable. Recent modeling work by Seman (1994) suggests that parcel descent in these conditions occurs on slant trajectories, follows the path of least resistance along the sloped isentropes, is directed back toward the generating convection, and takes place preferentially in the symmetrically unstable region. This coupling of the vertical updraft and slanted downdraft has been referred to as ''convective-symmetric instability'' (Conv-SI; Emanuel 1980; Seman 1991).

In his seminal paper discussing inertial stability and meridional motion in a circular vortex, Eliassen (1951) made some key points that are relevant to the current study. He noted the following.

> (a) In the gradient-balance, quasi-static theory, determining the meridional motion is not an initial value problem; the meridional motion depends only on the instantaneous sources of heat and angular momentum.
> (b) For a given heat or angular momentum source, stronger meridional motions develop the weaker the [inertial] stability of the vortex.
> (c) The meridional currents are assumed to be very slow compared to the vortex motion, so that the direct effect of the meridional circulation on the field of motion is slight. The importance of such weak meridional currents, however, does not lie in their direct effect on the wind field but in their ability to change profoundly the structure of the vortex by transporting the fields of the quasi-conservative properties of angular momentum and entropy.
> (d) The meridional streamlines are ellipses. The vertical extent of the ellipses is very small compared to their horizontal extent, and the major axis will in all cases be oriented approximately along the isentropic lines.

His results encouraged us to set up a model simulation and provide a simple (instantaneous) source of heating. The results also suggested that reduced inertial stability (produced by stronger jets) should provide a stronger response in the model.

In recent papers (Raymond and Jiang 1990; Raymond 1992; Seman 1994), in situ generation of potential vorticity anomalies was invoked to explain the upscale growth of convection into MCCs. In these studies, there were no regions of inertial instability (i.e., negative potential vorticity) before the onset of convection; local convection was responsible for the development of the inertial instability. Raymond and Jiang (1990) showed how the potential vorticity anomalies generated by an MCC itself can provide a mesoscale lifting mechanism to help maintain a convective system on mesoscale timescales. They argued that the net upward mass transport associated with the (relatively large-scale) convective heating within the system results in a negative (positive) potential vorticity anomaly at upper (lower) levels. With evaporation and melting of precipitation and thermal radiation, the low-level positive anomaly is strengthened, lifting the low-level isentropic surfaces further. Under favorable ambient vertical wind shear, low-level parcels approaching the MCC are forced to rise up the isentropic surfaces; if enough lifting occurs, conditional instability is realized. The convection, in turn, would act to reinforce the potential vorticity anomaly structure that caused it. It thus helps explain the longevity of an MCC after it has reached a relatively large size.

This model is very appealing because it can generate mesoscale jets (i.e., front-to-rear and rear-to-front flow) and both upper- and lower-level vortices within the MCS. It does not, however, address the question of why only some, instead of all, convective systems achieve this condition and grow upscale. A likely explanation lies in the work to be investigated here, where we address the following.

Hypothesis: *If the environment is predisposed to a state of weak inertial stability and convective instability, as suggested by the typical environments in which MCSs occur, then the divergent outflow from the upright convection at the equilibrium level can exploit the weak restoring force in the weakly inertially stable region and therefore be stronger and more persistent than otherwise. The result is continued stronger updrafts, lower-level perturbation pressure falls, and, eventually, the slant downdrafts suggested by CSI and Conv-SI theory. Further, the reduction of inertial stability results in less resistance to the growth of the convectively generated secondary circulations and the realization of an upper-level (low-level) negative (positive) potential vorticity anomaly. Specifically, if the mesoscale environment is already in a state of weak inertial stability, only small perturbations of this environment by convection may be required to render it inertially unstable. If the environment is already inertially unstable, the Conv-SI feedback process will occur quickly. Conversely, in an environment that is inertially very stable, the feedback process may never develop.*

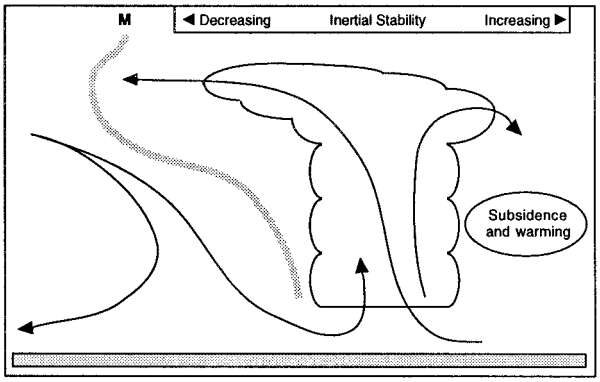

FIG. 2. Cross section in the *y–z* plane showing the conceptual model of trajectories of air parcels in inertially stable and unstable regions. In the inertially stable region (right side), outflow material descends in the near environment, resulting in drying and warming. The region of inertial instability (left side) permits meridional accelerations of outflow material. The thick, shaded line is a momentum (M) surface typical of inertially unstable regions. The vertical shear vector is directed into the page.

Figure 2 illustrates our conceptual model in the *y–z* plane. In the inertially stable region, the upper-tropospheric outflow is constrained by the balance of forces (i.e., Coriolis and pressure gradient forces), and subsidence takes place in the local environment, resulting in drying and warming. This tends to stabilize the atmosphere and suppress new convection. In the inertially unstable region where the forces are no longer in balance, parcels may be accelerated away from the local environment before subsidence occurs, allowing the convective instability to be maintained (Tripoli and Cotton 1989b). This meridional acceleration can advect the momentum field, as suggested by Eliassen (1951), such that inertially stable regions become less stable, leading to a positive feedback process. This enhancement of the divergence is partly a result of the change in Rossby radius when local angular momentum gradients are taken into account (Schubert et al. 1980). Anticyclonic regions will expand the Rossby radius and, consequently, the timescale of the geostrophic adjustment process. Figure 2 also illustrates how enhanced meridional transport, as a result of weak inertial stability, favors development of a larger and stronger solenoidal circulation. It is this circulation that is partially responsible for the continued generation of new convection through enhanced divergence aloft and convergence in the lower and middle troposphere.

Two points need to be made here. First, inertial instability is neither a necessary nor a sufficient mechanism to produce MCSs, but it is a process that aids in the growth of these convective systems. Second, symmetric instability, in which the role of static stability is taken into account (Xu 1986; Bjerknes 1951), may be regarded as isentropic inertial instability and it is appropriate to use the terms interchangeably.

Finally, it should be mentioned that the concept of inertial *stability* is often introduced into discussions of midlevel vortices observed in some MCSs (Menard and Fritsch 1989; Bartels and Maddox 1991), dynamic definitions of MCCs (Cotton et al. 1989), and tropical cyclone systems (Schubert and Hack 1982; Ooyama 1964, 1969; Charney and Eliassen 1964). The increase in inertial stability leads to a decrease in the forced secondary circulation and may play an important role in the maintenance of long-lived systems. We are concerned here, however, with an earlier stage in the MCS life cycle when upscale growth is dominant.

To explore the hypothesis that inertial instability plays a role in the development and evolution of mesoscale convection, we examined MCSs that occurred in 1) the data-rich PRE-STORM network and 2) environments sampled with new technology. Additionally, we used the Regional Atmospheric Modeling System (RAMS) developed at Colorado State University to simulate the conditions associated with weak inertial instability. The model experiments were analyzed to develop an understanding of the dynamics of this type of atmospheric motion and for comparison with the observational data.

3. Case studies

The current investigation was motivated by high-resolution observations taken during the PRE-STORM field program (Cunning 1986). Some mesoscale convective events observed during PRE-STORM occurred in regions that showed evidence of inertial instability prior to convection. It is useful to review those observations and others in light of our hypothesis about the role of inertial stability.

To assess the environmental conditions associated with mesoscale regions of inertial instability (or weak stability), we objectively analyzed rawinsonde data on isentropic surfaces. These data from the PRE-STORM field program had high temporal and spatial density. The ratio $\alpha = \eta_\theta / f$ was computed, where $\eta_\theta = \zeta_\theta + f$ is the isentropic absolute vorticity, ζ_θ is the isentropic relative vorticity, and f is the Coriolis parameter. A necessary condition for inertial instability is an environment in which $\alpha < 0$; days that satisfied this condition were selected for further investigation. PRE-STORM soundings were taken every 3 h during intensive operations periods (IOPs) and occasionally as often as every 1.5 h. Station spacing averaged approximately 200 km.

Twenty-one MCCs/MCSs occurred in the network during PRE-STORM, and 17 were during IOPs with special datasets. Of these, nearly 24% (4 of 17) of the MCC/MCS environments showed evidence of inertial instability; many others exhibited weak inertial stability. Analysis of the high quality data collected during the MCC that occurred on 12–13 May 1985 strongly suggests that the responses expected owing to an inertial instability were present. Data from three other PRE-STORM cases (6–7 May 1985, 16–17 June 1985, and

23–24 June 1985) are also suggestive, but they are not as complete as those of 12–13 May 1985.

A second source of high quality data is the Mesoscale Analysis and Prediction System (MAPS; Benjamin et al. 1991; Benjamin et al. 1996).[1] Analysis output was used to select a large set of MCC events on the basis of the presence of inertial instability prior to convection.

We discuss two cases that are representative of each data type: one from the PRE-STORM field program using high-temporal and -spatial-density soundings, and one using high-resolution gridded model data from MAPS. Additional PRE-STORM and MAPS case studies were discussed by Blanchard (1995).

a. PRE-STORM case: 12–13 May 1985

The mesoscale convective event that occurred on 12–13 May 1985 is one of only three during PRE-STORM in which upper-air soundings were released *before* the onset of convection, allowing an examination of the preconvective environment for conditions that were important to the subsequent development of the MCC. This MCC originated as a broken line of convective cells oriented northeast–southwest (Fig. 3a) along a quasi-stationary ''secondary'' dryline (Schaefer 1986). Later, a mesoscale band of convection developed that was oriented northwest–southeast and moved to the northeast. During the transition from one orientation to the other (Figs. 3b,c), there were short, weak lines of convection having this northwest–southeast orientation superimposed on the original line of convection. The original northeast–southwest line of convection weakened while the northwest–southeast line continued to evolve and produce copious amounts of stratiform precipitation;[2] stratiform precipitation was not an important feature of the original dryline convection. The development of strong convection quickly followed by stratiform precipitation was similar to that described by McAnelly and Cotton (1992).

Figure 4 is a satellite image taken at 0100 UTC 13 May 1985 that clearly shows the developing MCC in Oklahoma and a second area of strong convection in northern Texas. Figure 5 is a composite chart depicting conditions at 0000 UTC 13 May 1985 at 500 mb with surface fronts and pressure centers superimposed. The synoptic-scale trough over the west was moving eastward toward the plains. A surface front was oriented east–west near the Oklahoma–Kansas border, and a dryline was in western Oklahoma; a secondary dryline was in central Oklahoma. Weak cyclonic vorticity was located to the southwest of the PRE-STORM network ahead of the approaching short wave. Convection began during the afternoon in southwest Oklahoma and produced numerous severe thunderstorms; subsequent storms formed in central and northeast Oklahoma. These storms were not as severe and eventually evolved into the MCC. A mesoscale jet streak with winds greater than 60 m s^{-1} was observed over west-central Kansas at 0000 UTC and resulted in a region of strong anticyclonic shear. Figure 6 shows values of $\alpha = \eta_\theta / f$ on the 330-K isentrope; negative values indicate regions of inertial instability. The depth of this unstable layer is shown in the vertical cross section in Fig. 7. It should be clear from these two figures that there is a large region, both horizontally and vertically, that is inertially unstable.

Along with examining fields at a specific time, it is also useful to look at the temporal changes in these scalar and vector fields and determine how the changes may be related to the instability. By computing the difference in the winds between 0000 and 0300 UTC, we can determine the local rate of change of the wind $\delta\mathbf{V}/\delta t$, where $\mathbf{V}$ is the observed wind. The vector change of the wind was examined for many levels (not shown). At low levels (e.g., 308-K isentrope, ranging from about 825 mb in the south to 600 mb in the north), there was an increase in the southwesterly flow south and east of the convective system and northerly flow north of the convective system. At the upper level (330 K; approximately 300–230 mb), the accelerations over Oklahoma were generally upshear toward the west; over Kansas they were divergent and directed toward the northwest through the northeast. The strength of the 3-h changes over Kansas, and their asymmetry and orientation, suggest developing divergent outflow through the region of the inertial instability. Inspection of animated satellite imagery clearly shows that portions of the spreading anvil moved across the mean flow; that is, the anvil spread to the north and northwest in a region where the large-scale flow was from the southwest at speeds of approximately 20–30 m s^{-1}.

To gain insight into where the air parcels were descending, let us examine Fig. 8, which shows the change in geopotential height, temperature, dewpoint, and wind at Enid, Oklahoma (END). END is located on the southern edge of the region of inertial instability and is within the region where the northwest–southeast-oriented convective bands developed. Above about 400 mb, the local rate of change of the wind is from the east-southeast, whereas below that level it is from the north to northeast. There is a positive height change that peaks at 200 mb that is very likely associated with the spreading anvils from convection; from 275 to 800 mb there is a negative height change.[3] There is slight warming in a deep layer

[1] Currently available from the National Centers for Environmental Prediction (NCEP) as the Rapid Update Cycle (RUC).

[2] C. A. Doswell (1995, personal communication) has shown that what is typically referred to as stratiform precipitation in MCSs is really convective in structure, albeit with weak horizontal gradients in intensity.

[3] Recall that the geopotential height is computed from the virtual temperature and reflects the combined changes in the temperature and moisture.

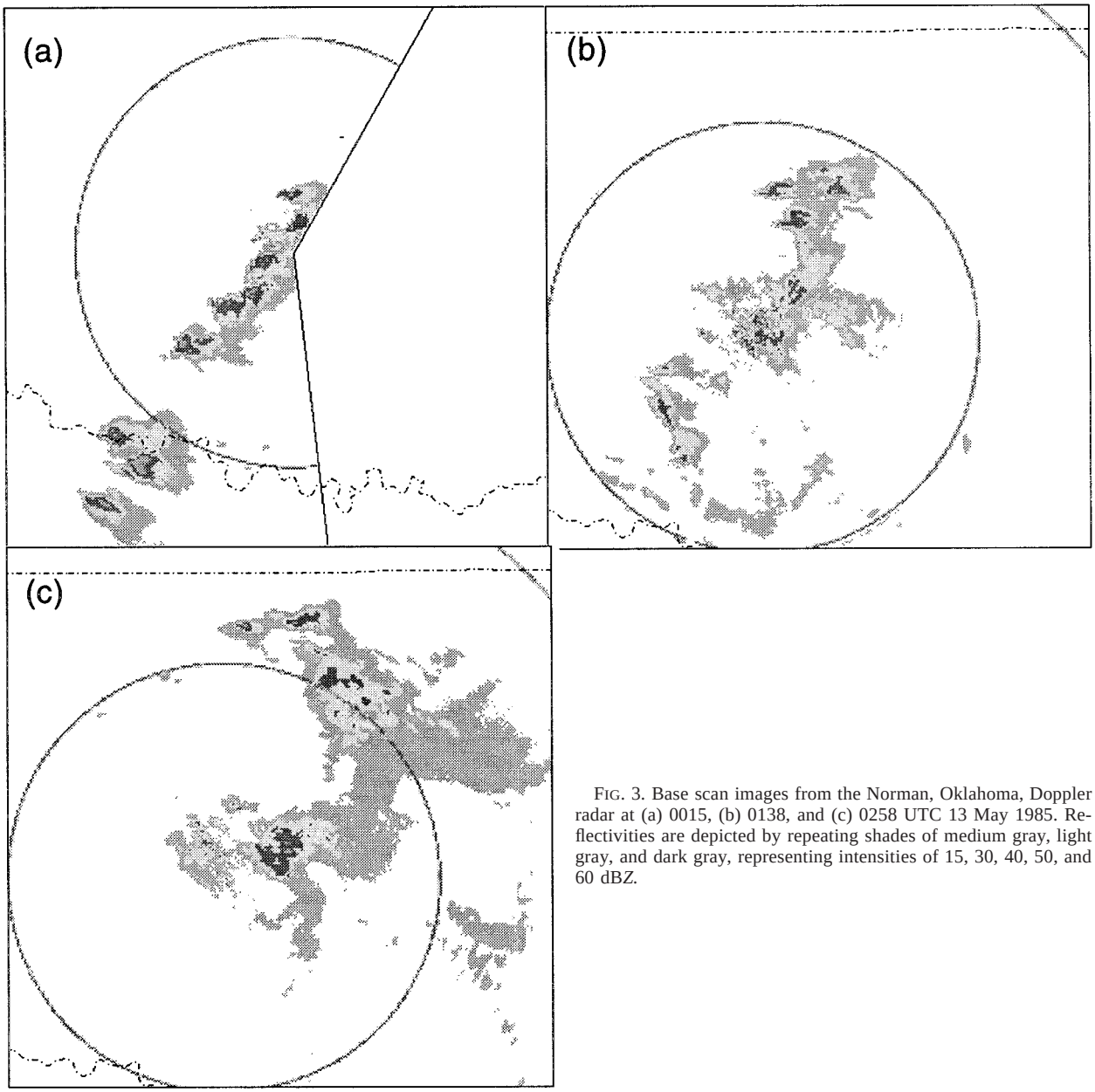

FIG. 3. Base scan images from the Norman, Oklahoma, Doppler radar at (a) 0015, (b) 0138, and (c) 0258 UTC 13 May 1985. Reflectivities are depicted by repeating shades of medium gray, light gray, and dark gray, representing intensities of 15, 30, 40, 50, and 60 dBZ.

below the anvil level; the moisture shows a drying trend in the same layer. What is probably happening here is outflow from the strong, upright convection is accelerating preferentially to the north and northwest. If a secondary mesoscale circulation such as depicted to the left of the convection in Fig. 2 exists, we might expect a flow from the northwest at lower levels. That the observed flow is more northerly may partly be a consequence of more rapid geostrophic adjustment of this lower branch in the region of greater inertial stability at lower levels.

Finally, we examine some basic quasigeostrophic analyses as part of our effort to diagnose the cause of the evolution of the convection into a mesoscale system. Figure 9 shows the diagnosed vertical structure of the divergence of the **Q** vector (Hoskins et al. 1978; Hoskins and Pedder 1980; Barnes 1985). The **Q** vector is defined as

$$\mathbf{Q} = \left[\frac{\partial \mathbf{V}_g}{\partial x}\cdot\nabla\left(\frac{\partial\Phi}{\partial p}\right), \frac{\partial \mathbf{V}_g}{\partial y}\cdot\nabla\left(\frac{\partial\Phi}{\partial p}\right)\right], \qquad (1)$$

where Φ is the geopotential height and $\mathbf{V}_g$ is the geostrophic wind. The divergence of **Q** is related to the quasigeostrophic ascent through

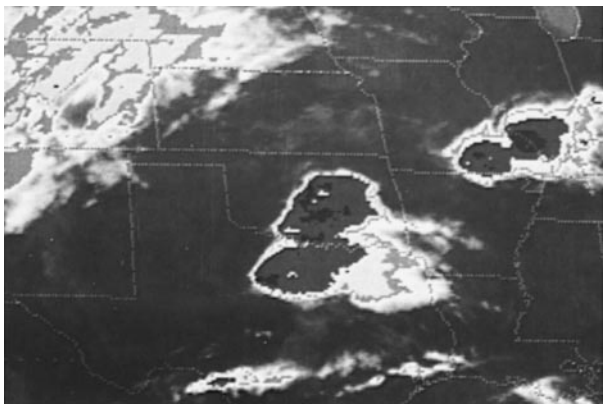

FIG. 4. Satellite infrared image taken at 0100 UTC 13 May 1985. The developing MCC can be seen in Oklahoma at this time.

$$\sigma\nabla^2\omega + f_0^2\frac{\partial^2\omega}{\partial p^2} = -2\nabla\cdot\mathbf{Q}, \qquad (2)$$

where σ is the static stability, ω is the vertical velocity, and f_0 is the mean Coriolis parameter. The cross section in Fig. 9 is from the northwest to southeast and bisects the PRE-STORM network. The shaded areas correspond to areas of **Q** vector convergence and represent regions of upward forcing. The PRE-STORM network is located about one-quarter of the way from the right-hand edge and is favored by strong upward forcing. It can be argued that the ensuing convection and upscale growth into an MCC are related entirely to quasigeostrophic adjustments and not to inertial instability. However, if this were true, then the convection that developed farther south in the region of inertial *stability*, but still in the region of upward forcing, should have also been favored to grow upscale. In fact, the convection in northern Texas began to dissipate after sunset while the convection in the PRE-STORM network continued to grow. Although the ageostrophic circulations required to maintain hydrostatic and quasigeostrophic balance very likely played a significant role in preparing the environment for convection by thermodynamically destabilizing and moistening the atmosphere, it is suggested that the presence of the inertial instability allowed one region of convection to grow upscale into a mesoscale system while others dissipated.

b. MAPS case: 13–14 May 1992

To increase the number of instances of either weak inertial stability or inertial instability, we collected data from a number of convective events that occurred during the warm season of 1992. These events were analyzed with model data from MAPS, a four-dimensional data assimilation system using a hybrid sigma–isentropic vertical coordinate system that is ideal for the analysis required in this study. Horizontal resolution for the domain was 60 km and vertical resolution was 4–8 K. MAPS takes advantage of all available data types, including rawinsonde data, surface data, wind profiler data, and wind and temperature data from commercial airliners. Consequently, MAPS is often able to analyze features that are too small in scale to be handled properly by other models. It is for these reasons that data from

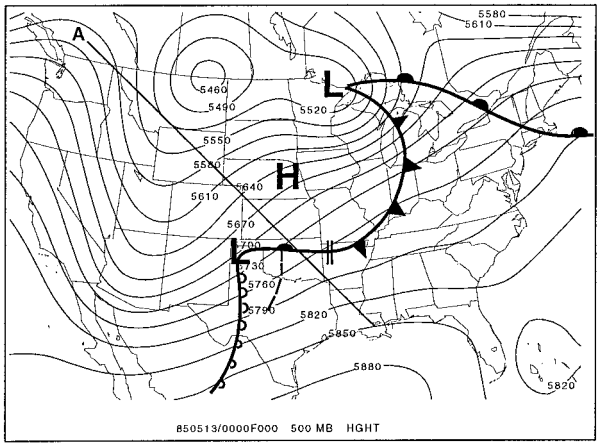

FIG. 5. Composite chart at 0000 UTC 13 May 1985 depicting conditions at 500 mb with surface fronts and pressure centers superimposed. The 500-mb height contour interval is 30 m. High and low pressure centers marked with H and L, respectively. Surface boundaries use standard conventions for cold and warm fronts, the dry line, and surface pressure troughs. The line labeled A denotes the cross section shown in Fig. 9.

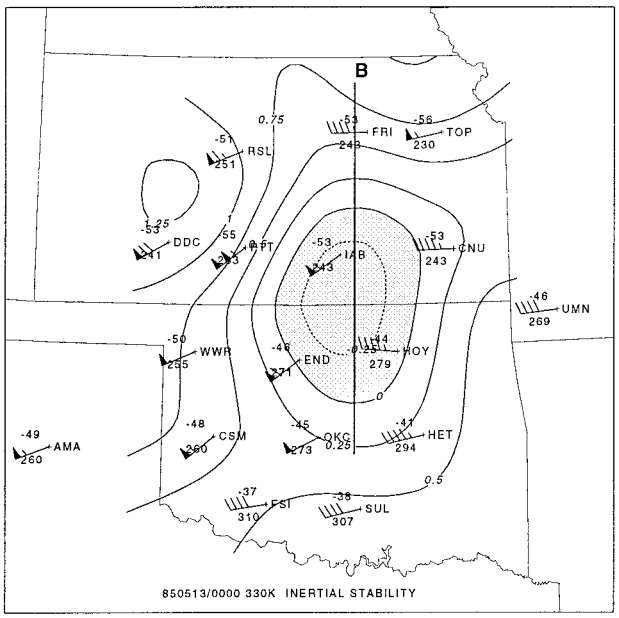

FIG. 6. Plan view (x–y plane) of the inertial stability parameter, defined as $\alpha = \eta_\theta/f$, where $\eta_\theta = \zeta_\theta + f$, over the PRE-STORM network on the 330-K isentrope at 0000 UTC 13 May 1985. The contour interval is 0.25. Positive values are shown by solid lines; negative values, dashed and shaded. Each station plot shows temperature (upper; °C) and pressure (lower; mb). Winds are shown with the half-barb equal to 2.5 m s^{-1}; full barb, 5.0 m s^{-1}; and pennant, 25 m s^{-1}. The line labeled B denotes the cross section shown in Fig. 7.

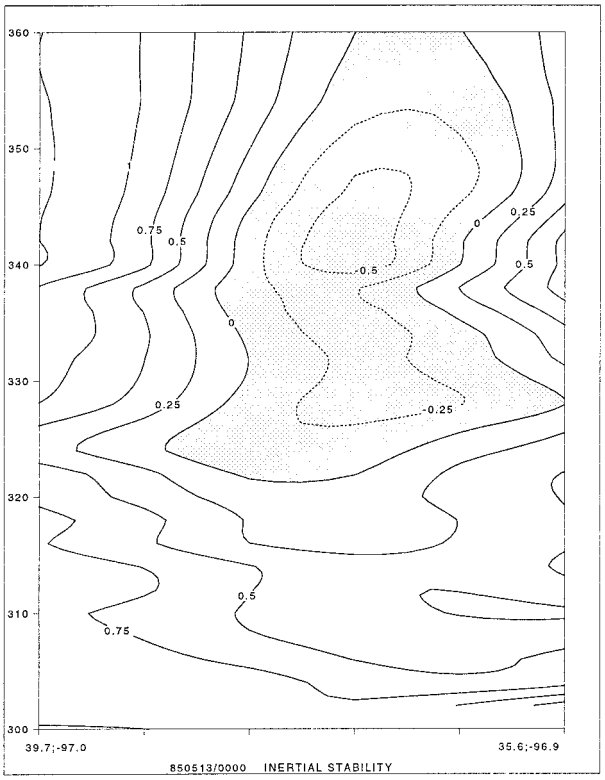

FIG. 7. Vertical cross section of the inertial stability parameter α at 0000 UTC 13 May 1985. The cross section extends from the north-central to the south-central portion of the mesonetwork (line B in Fig. 6). The contour interval is 0.25. Positive values are shown by solid lines; negative values, dashed and shaded. The latitude and longitude of the cross section endpoints are plotted in the lower-left and lower-right corners. Ordinate is potential temperature θ; tick marks are every 10 K.

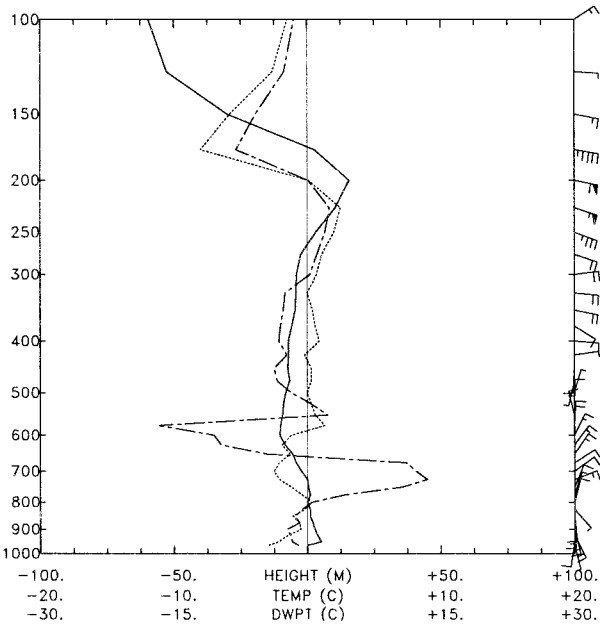

FIG. 8. Vertical profile of changes between 0000 and 0300 UTC 13 May 1985 in the height (solid), temperature (dotted), dewpoint (dashed), and vector change (right axis) in the wind for Enid, Oklahoma (END). The scale for each parameter is at the bottom. The wind plotting convention is as in Fig. 6.

MAPS analyses (not forecasts) were used to investigate features associated with MCSs occurring in regions of weak inertial stability.

The mesoscale convective events that occurred during the night of 13–14 May are interesting because two large MCSs formed during the evening hours: one developed along the Nebraska–Kansas border and the other formed in central Texas. Both systems occurred in regions of weak inertial instability. The northern system was one of the largest MCCs during 1992. Figure 10 is an infrared satellite image at 0000 UTC 14 May 1992. The southern system in Texas is weakening at this time and covers only a small fraction of its largest areal extent approximately 3 h earlier. The northern system is just beginning to take on mesoscale characteristics. The original convection consisted of isolated thunderstorms in an arc from the South Dakota–Nebraska border south and southwest to the Kansas–Colorado border. Figure 11 is a composite chart showing 500-mb height contours and the location of surface fronts, highs, and lows. Aloft, troughs are present over both the west and east coasts, whereas in higher latitudes a pair of short-wave troughs are situated over the Great Lakes and approaching the northern High Plains. The north–south portion of the surface front, backed up against the eastern slope of the Rocky Mountains, was quasi-stationary. The surface high pressure shown over the Great Lakes produced a southeasterly return flow over the western plains and was responsible for advecting low-level moisture back into the region.

Three-hourly MAPS analyses were used for this case. The analysis at 0000 UTC 14 May 1992 is revealing (Fig. 12). The inertial stability parameter α shows a region of weak inertial instability over Nebraska, extending both to the southwest and east. This area of inertial instability corresponds to the region in which the initial convection started and evolved upscale into the MCS. Another region of inertial instability, located along the Texas–Oklahoma border, was also associated with long-lived convection. Inspection of the available data suggests that this region of instability may be, at least in part, the result of the earlier convection over Texas.

A cross section of the MAPS analysis gridded data provides further insight into the environment (Fig. 13). The cross section was taken from northwest South Dakota to north-central Kansas. Along this cross section, the initial convection occurred in a region where inertial instability was present aloft embedded in a larger region of weak inertial stability and was bounded on the south by a region of high inertial stability. In this particular event, upright convection dominated, and the probable role of any slant downdrafts along the CSI/Conv-SI-induced solenoid was to return air parcels diverging

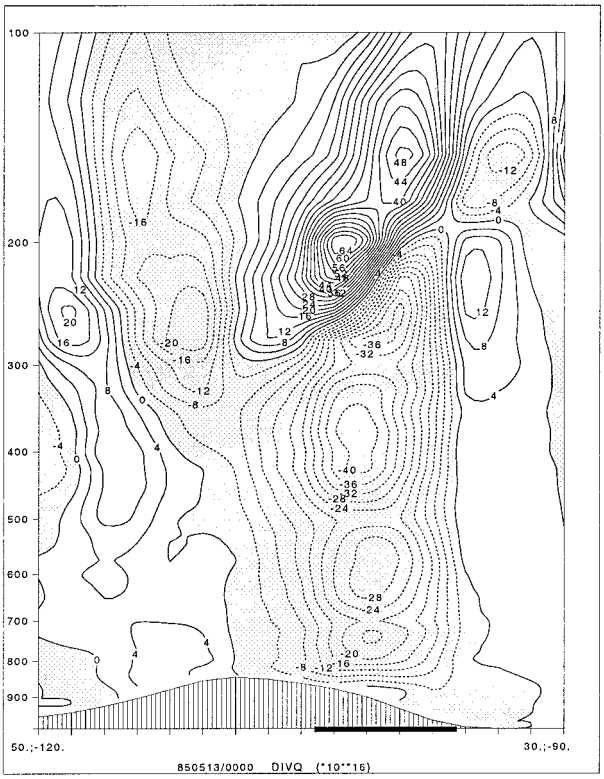

FIG. 9. Northwest–southeast vertical cross section (line A in Fig. 5) at 0000 UTC 13 May 1985 of the divergence of the **Q** vector (contour interval, 4×10^{-16} m^2 kg^{-1} s^{-1}). Solid lines are positive values; dashed lines, negative. The region of **Q** vector convergence, implying upward forcing, is shaded. The PRE-STORM network is marked by the heavy bar at the bottom. Latitude and longitude are plotted as in Fig. 7.

from the anvil regions of the convection back down to lower levels.

c. Composites: 1990–93

Recently, J. A. Augustine (1995, personal communication) composited rawinsonde data from many MCSs during the period 1990–93. His compositing technique is similar to that used by Maddox (1983) and Cotton et al. (1989) and was described by Augustine and Caracena (1994). The method assures that there is little or no convection occurring in the region of interest that would contaminate the rawinsonde data with a convective signature. MCS cases were divided into ''large,'' ''small,'' and ''nondeveloping'' events. Large MCSs were those that qualified as MCCs (Maddox 1980)—that is, those that attained at least 100 000 km^2 at maximum areal extent (defined by the cloud-top area less than or equal to -32°C). Small MCSs were defined as those that did not satisfy large MCS or MCC criteria but were large enough at maximum areal extent to be considered multi-

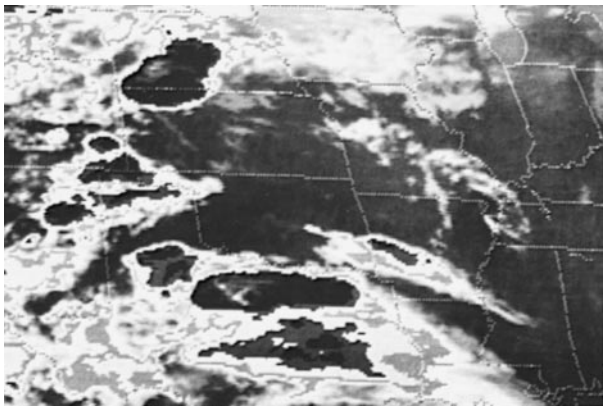

FIG. 10. Satellite infrared image taken at 0000 UTC 14 May 1992. The developing MCC can be seen in western Nebraska.

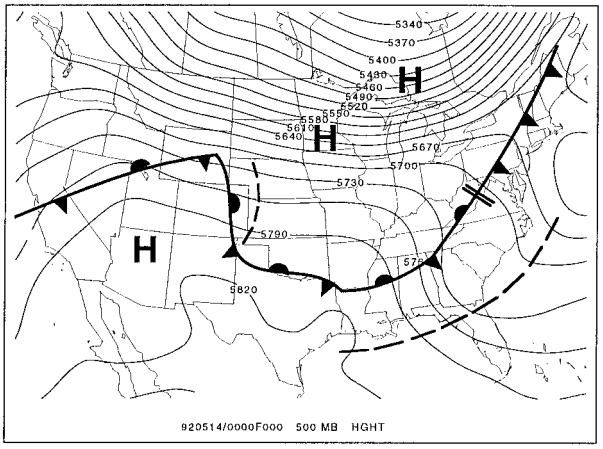

FIG. 11. As in Fig. 5 except for 0000 UTC 14 May 1992.

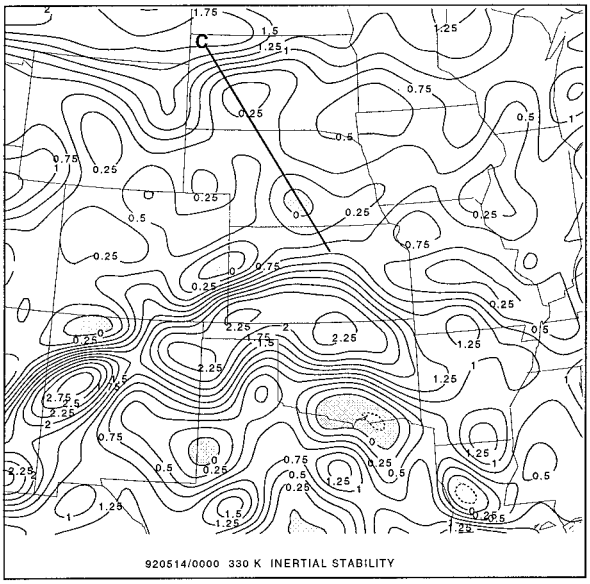

FIG. 12. The inertial stability parameter α on the 330-K isentrope for 0000 UTC 14 May 1992. The contour interval is 0.25. Positive values are shown by solid lines; negative values, dashed and shaded. The line labeled C denotes the cross section shown in Fig. 13.

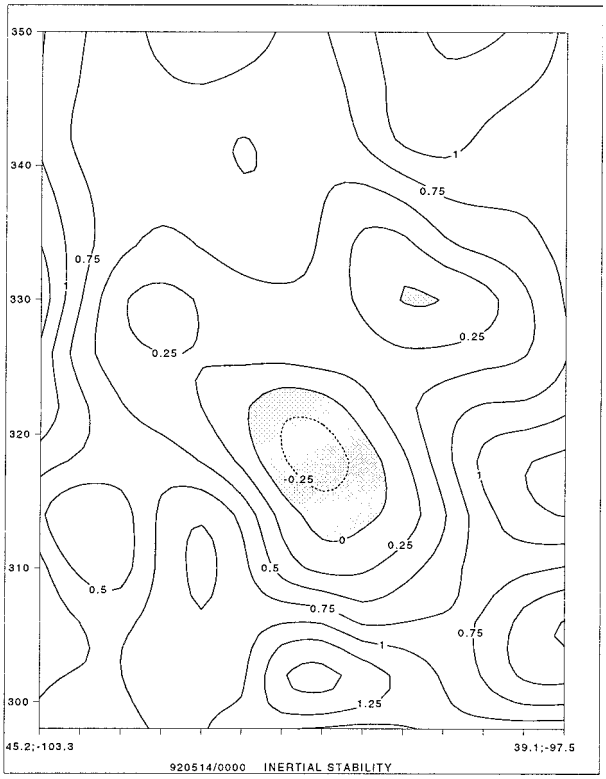

FIG. 13. Vertical cross section of the inertial stability parameter α (contour interval, 0.25). The cross section extends from northwest South Dakota to north-central Kansas (line C in Fig. 12). Positive values are solid lines; negative values, dashed and shaded. Latitude and longitude are plotted as in Fig. 7. Vertical coordinate is potential temperature θ; tick marks are every 10 K.

cell thunderstorm complexes. The nondeveloping class comprised the remainder of the cases in which convection did not grow upscale to meet the small or large classification. After the rawinsonde data were composited, the results were analyzed using the analytic approximation technique of Caracena (1987).

At 200 mb, Augustine's composites for large MCS cases show that there is a strong north–south gradient in the wind speed (Fig. 14a), similar to that shown by Maddox (1983) and Cotton et al. (1989). The Caracena (1987) analysis scheme, however, preserves the gradient of the north–south wind speeds better than is typical in other analysis schemes. Augustine also computed the inertial stability and obtained values less than 0.7 for large MCSs. Note, in particular, that the large MCS genesis location (denoted by the $\otimes$) is in this well-defined region of minimum values; a strong gradient of inertial stability is located north of this region. On the other hand, the nondeveloping convective systems are in regions where the inertial stability is greater ($\alpha \approx$ 0.8: Fig. 14b) and are located in a strong east–west gradient of inertial stability.

Even though the values associated with the large MCSs are more stable than the values realized in the individual case examples above, it must be understood that Augustine's results are for composites of many events. In that light, his results are very revealing about the nature of the upper-level flow associated with MCSs and clearly show that there is a broad region of weak inertial stability associated with the preconvective genesis region of MCSs. This suggests that the weak inertial stability may have played an important role in the development and maintenance of persistent cross-contour

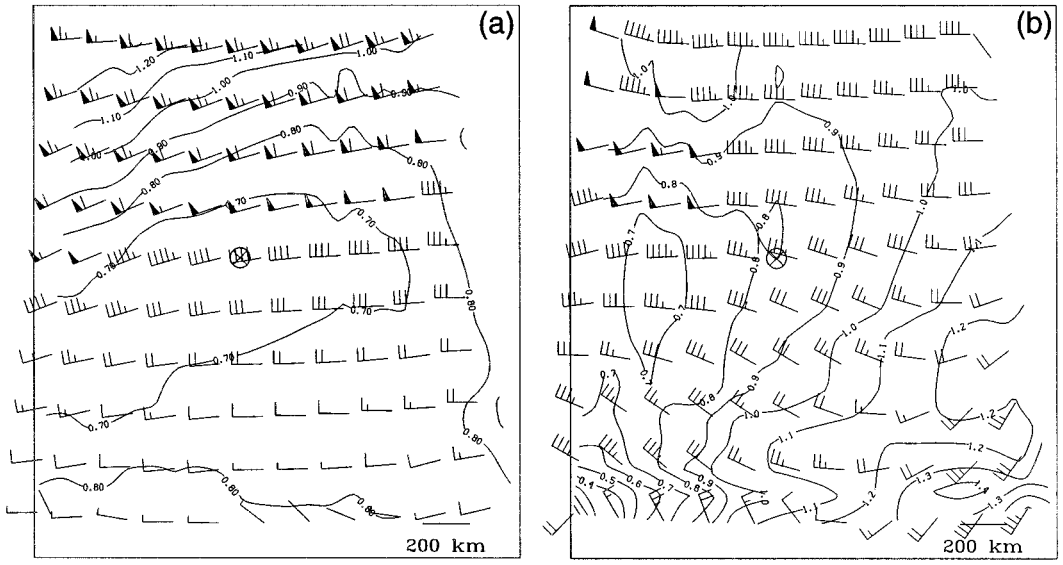

FIG. 14. Composite of mesoscale convective events depicting the large-scale environment associated with (a) large MCSs and (b) nondeveloping convective systems, at 200 mb. Contours (every 0.10) represent inertial stability. Winds are as in Fig. 6. The location of MCS genesis is marked by $\otimes$. Figure courtesy of J. A. Augustine (NOAA/Air Resources Laboratory).

outflow in the large MCSs; the presence of stronger inertial stability may have minimized the cross-contour outflow in the nondeveloping convective systems.

4. Design of numerical model experiments

To examine the processes that are responsible for the solenoidal circulations, and as a preliminary step toward assessing the potential these circulations have for causing upscale growth of convective systems, we performed numerical experiments using a nonhydrostatic mesoscale model. The intent was to explore the importance of the initial distribution of $\alpha = \eta/f$ (where $\eta = \zeta + f$) and strengths of heating by convection on the evolution of MCSs and the upper-level divergent outflow. Because our focus is on the strength and structure of the solenoidal flow forced by the convection rather than on the convection itself, and for ease of interpretation, we represent the convection by an imposed mesoscale time-dependent heating function.

a. RAMS model description

The model used in this study was the Regional Atmospheric Modeling System (RAMS) developed at Colorado State University. RAMS is a nonhydrostatic, primitive equation model that is highly flexible and modular, with many possible configurations. It has been described extensively in the literature, most recently by Pielke et al. (1992). The reader is referred to the original papers for complete documentation of the model and to Blanchard (1995) for additional details on the configuration used in this study.

The nonhydrostatic version of RAMS was used, in which u, v, and w wind components, ice and liquid water equivalent potential temperature, dry air density, total water mixing ratio, and the mixing ratios of the various water variables are predicted. From these variables, pressure, potential temperature, temperature, vapor mixing ratio, and cloud water mixing ratio are diagnosed.

All the experiments were two-dimensional with a vertical domain of 40 grid points with 600-m resolution, giving a depth of about 23 km. The horizontal domain had 200 points with 5-km resolution, resulting in a cross section of 1000 km. The cross section was oriented east–west; this is the standard configuration for 2D planes in RAMS. This configuration with constant Coriolis force is the equivalent of a north–south cross section on an f plane. Accordingly, the cross section can be viewed in either framework.

The vertical velocity was constrained to be zero at the top boundary. This condition is simple, but has the disadvantage of causing strong reflection of upwardly propagating gravity waves. Consequently, a Rayleigh friction absorbing layer was used in the top six levels. The friction layer is designed to absorb gravity waves approaching the lid, sufficiently damping them before and after reflection so that they are effectively eliminated. Lateral boundaries use the Klemp and Wilhelmson (1978) condition in which the normal velocity component specified at the lateral boundary is effectively advected from the interior, assuming a propagation speed (intended to be similar to a dominant gravity wave phase speed) of 20 m s^{-1}. The lateral boundary values of each variable other than the normal velocity component are set to the value in the field immediately adjacent to the boundary in the interior, that is, a zero-gradient condition.

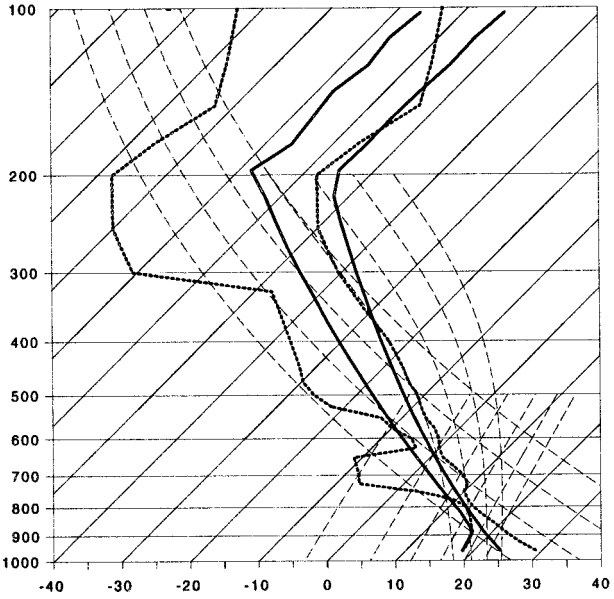

FIG. 15. Skew T–ln$p$ diagram of the two soundings used in the model experiments. The short-dashed lines are a slightly smoothed version of the temperature and moisture profiles from the Oklahoma City (OKC), sounding taken at 0000 UTC 13 May 1985. The solid lines are the temperature and moisture profiles from the Weisman–Klemp (WK) idealized model sounding.

b. Initialization

The model was initialized using a typical midwestern springtime sounding (Fig. 15) taken prior to a large convective event. We chose to use a slightly smoothed version of the Oklahoma City, Oklahoma, sounding from the PRE-STORM case study discussed in section 3 (0000 UTC 13 May 1985). RAMS requires that 2D integrations use a horizontally homogeneous initialization. Further, the Coriolis force does not act on base-state winds in 2D integrations; any initial horizontal wind is implicitly assumed to be horizontally uniform and in geostrophic–thermal wind balance. Thus, it was necessary to create the jet as a perturbation on the base state, which was taken as a state of rest. This was accomplished by starting the integration and activating a forcing function for the wind. The function had the form

$$F_v = V_0 \exp[-x_j^2(x - x_0)^2] \exp[-z_j^2(z - z_0)^2], \quad (3)$$

where V_0 is the amplitude of the imposed acceleration

[m s^{-1} (72 h)$^{-1}$] and x_j and z_j are shape parameters for the horizontal and vertical components of the jet. This forcing function was allowed to operate for 72 h to allow slow increases in the wind and to keep the wind and temperature responses in approximate thermal wind balance. After the initial 72-h spinup period, the integration was suspended. The results were saved in a history file and used as initial conditions for the numerical experiments discussed later in this section.

Considerable effort was made to determine an appropriate strength for the jet and resulting values of inertial instability. Not surprisingly, it was found that as long as the absolute vorticity[4] η, remained positive, the jet was stable with time. On the other hand, if the absolute vorticity became negative during spinup, an adjustment process triggered by the instability became evident. This manifested itself as a vertically stacked set of strong, horizontal accelerations of alternating sign having a spacing of $2\Delta z$ giving a vertical wavelength of $4\Delta z$. The appearance of inertial instabilities on small scales has been described by Stevens and Cielsielski (1986), who showed that the shallow modes should grow the fastest in the absence of vertical diffusion. A series of sensitivity experiments indicated that for large jet values (and large degrees of inertial instability with values of $\alpha = \eta/f \approx -0.6$), the adjustment process would begin even before the 72-h spinup process was complete. Moderate jets ($\alpha \approx -0.4$) resulted in an adjustment process becoming prominent approximately 4 h after the spinup process was complete. Weaker jets ($\alpha \approx -0.2$) did not show significant signs of instability until after 6 h beyond the end of spinup. The jet strengths were selected so that $\alpha \geq -0.2$, resulting in environments that were ''weakly inertially unstable'' to ''weakly inertially stable.''

Imposed heating, applied only after the 72-h spinup period, has the form

$$F_H = H_0 \exp[-x_H^2(x - x_0)^2] \exp[-z_H^2(z - z_0)^2], \quad (4)$$

where H_0 (°C h^{-1}) is the amplitude, and x_H and z_H are shape parameters. This forcing function is similar to that employed by Hertenstein and Schubert (1991) in their study of potential vorticity anomalies with squall lines. Nicholls et al. (1991), Bretherton and Smolarkiewicz (1989), and Mapes (1993) have used similar, idealized heating models and have shown that such simplified analytical solutions capture a number of realistic features of thermally forced gravity waves that have been simulated in more complex models. This forcing function was allowed to increase from zero to full strength over a period of 1 h, approximating the actual heating taking place due to convection when averaged over a meso-β-scale domain. The ''ramp up'' was of the form

$$F_{H^*} = F_H \sin^2\left(\frac{\pi}{2}\delta t\right), \qquad 0 \leq t \leq \delta^{-1}, \quad (5)$$

where t is the time in seconds and δ was set to the inverse of the ramp-up time, for example, (3600 s)$^{-1}$ for a 1-h ramp. The values of x_H and z_H were chosen so that the heating had meso-β-scale dimensions ($\sim$175 km) in the horizontal and peaked at around 7 km in the vertical. That is to say, the heating was intended as a representation of the mesoscale aggregate of many individual convective cells. Heating rate H_0 of 1°, 3°, and 5°C h^{-1} correspond to precipitation rates of approximately 0.15, 0.45, and 0.75 cm h^{-1}. These precipitation rates are small if we consider convective precipitation, but are typical values for an average precipitation rate over large areas (Churchill and Houze 1984; Leary 1984; McAnelly and Cotton 1986, 1989; Johnson and Hamilton 1988). All experiments were run for an additional 5 h after ramp up (i.e., to the end of the integration) with F_H held constant.

c. Model configuration

The RAMS numerical mesoscale model is capable of simulating many features of the atmosphere. Although it would have been possible to perform the experiments discussed here using 3D grids, full microphysics, radiation, complex surface processes, and other features, the decision was made to proceed with the simplest configuration possible. All integrations were done in 2D, no latent heating was allowed, and both short- and longwave radiation schemes were turned off. Although this configuration does not adequately simulate the myriad of complicated physical processes occurring in real MCSs, it has the benefit of isolating the fundamental role of inertial instability on the development of enhanced divergence aloft and secondary circulations necessary for the upscale evolution of convection into MCSs.

Another issue that needs to be addressed is the applicability of a 2D experiment, as opposed to a full 3D experiment. Note that although the experiments occur in the *x–z* plane,[5] the wind shear is in the *meridional* direction, perpendicular to this plane such that the ambient meridional wind is parallel to the axes of the circulations that develop. This is different from many 2D simulations in which basic-state shear is in the plane of the simulations (e.g., Thorpe et al. 1982; Rotunno et al. 1988; Tripoli and Cotton 1989a; Fovell 1991). The ge-

[4] RAMS computes kinematic fields on σ_z surfaces, which reduces to simple *z* surfaces in the current model configuration. The absolute vorticity on a *z* surface, hereafter referred to as η, is qualitatively very similar to η_θ but may be underestimated by 5%–10% in regions of steep isentropic slope.

[5] As discussed earlier, the domains of these simulations are oriented east–west but can also be described as north–south domains on an *f* plane. Thus it is appropriate to replace *x–z* with *y–z* and *meridional* with *zonal* in the discussion that follows.

TABLE 1. Values for fixed parameters used in RAMS.

Parameter	Value
Horizontal shape parameter of the jet, x_J	160 km^{-1}
Vertical shape parameter of the jet, z_J	4 km^{-1}
Spinup time for the jet	72 h
Horizontal shape parameter of the heating, x_H	40 km^{-1}
Vertical shape parameter of the heating, z_H	3 km^{-1}
Ramp time for the heating	1 h
Level of maximum heating	7 km
Horizontal resolution	200 points; 5 km
Vertical resolution	40 points; 600 m

ometry is set up this way so that the cross-stream ageostrophic secondary circulations produced by the combined dynamical effects of baroclinity, static stability, and Coriolis deflection can be studied. This geometry is essentially the same as that employed by Seman (1990, 1994) in his study of Conv-SI. With this geometry, the rotational component of the wind is completely described by the v component, and the divergence is completely described by the u component of the wind.

Because we are investigating the possibility that inertial instability can increase the divergent cross-stream flow, and we designed our experiment so that the jet is into the 2D domain, only the east–west wind component is affected by changes in the inertial stability. Thus, the 2D formulation greatly simplifies the problem while retaining the essential information for analysis and interpretation.

5. Results of numerical modeling experiments

The RAMS model experiments were executed with different jet strengths to test the sensitivity of the response to the strength of the inertial instability (as suggested earlier in section 2), and with heating functions of various intensities. To provide a baseline for the comparison of results, we also discuss a control experiment without a jet core. Additional experiments were conducted to determine the role of latitude, ambient static stability, and vertical shear.

Certain parameters were fixed for all experiments and are shown in Table 1; variable parameters are listed in Table 2. As can be immediately seen from Table 2, there are four wind speeds, three heating rates, and two latitudes being tested, giving a total of 24 experiments. An additional three experiments (5–7) were conducted to determine the role of static stability and vertical shear.

a. Control experiments (1a–f)

Experiment 1b imposes the heating function (H_0 = 3°C h^{-1}) without any jet in the domain. The field of potential temperature θ is then horizontally homogeneous when the heating is turned on. After 1 h (total integration time is now 73 h; all references to model integration time will be relative to the restart time at 72 h), weak horizontal winds have developed in response to the vertical motions from the forced heating. The u component of the wind (hereafter u wind) has a maximum speed of about $\pm$1.3 m s^{-1} and diverges symmetrically away from the (vertical) axis of maximum heating. Coriolis turning of this outflow is already manifested as weak anticyclonic flow aloft. After 2 h, the u winds have continued to increase in strength and have peak values of $\pm$3.7 m s^{-1}. This increase in speed continues and after 3 h has peak values of $\pm$5.1 m s^{-1}.

By the end of the integration at 6 h, the u winds (Fig. 16a) have attained speeds of close to $\pm$6.0 m s^{-1}. The v winds (Fig. 16b) have peaked at $\pm$6.0 m s^{-1} and are directed into the domain on the left side of the heating, and out of the domain on the other side, clearly indicating the development of an anticyclone above the heating. Figure 16c shows the total vorticity ($\zeta + f$) associated with the rotational component of the wind (the v wind, in this case). Two areas of negative vorticity exist adjacent to the top of the updraft and are related to the generation of the rotational v winds that are displaced laterally from the updraft core; outside this region, the vorticity is strongly positive. This in situ generation of negative absolute vorticity has been discussed

TABLE 2. Characteristic values for the jet and heating profiles and variable latitudes used in the model experiments. Here, V_0 [appearing in Eq. (3)] has been multiplied by 72 h to put it in units of velocity.

Experiment	Winds, V_0 (m s^{-1})	Heating, H_0 (°C h^{-1})	Latitude (deg)	Experiments/comments
1a–c	0	1; 3; 5	40	Control experiments
1d–f	0	1; 3; 5	25	
2a–c	10	1; 3; 5	40	Moderate inertial stability
2d–f	10	1; 3; 5	25	
3a–c	20	1; 3; 5	40	Weak inertial stability
3d–f	20	1; 3; 5	25	
4a–c	30	1; 3; 5	40	Weak inertial instability
4d–f	30	1; 3; 5	25	
5	30	3	40	Increased vertical stability
6	30	3	40	Base-state vertical shear
7	0	3	40	Base-state vertical shear; no jet

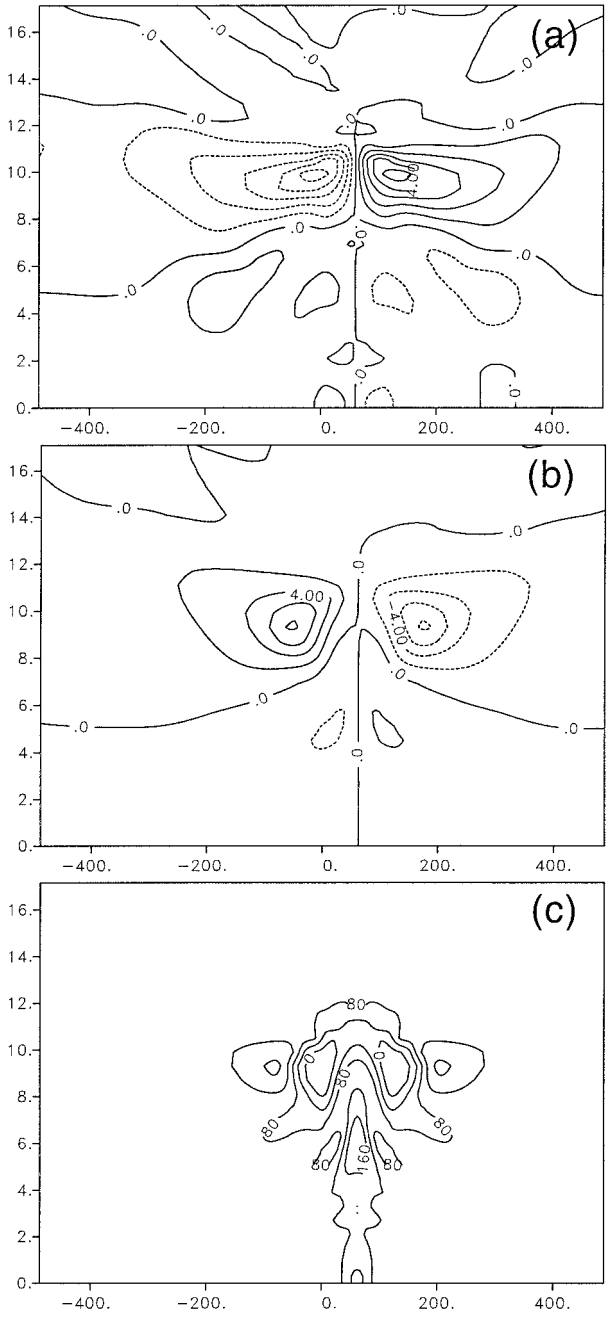

FIG. 16. Vertical cross section at $t = 6$ h for experiment 1b for (a) the u component of the wind (contour interval, 1.0 m s^{-1}; negative values, dashed), (b) the v component of the wind (contour interval, 2.0 m s^{-1}; negative values, dashed), and (c) absolute vorticity $\eta = \zeta + f$ (contour interval, 40×10^{-6} s^{-1}; negative values, dashed). The horizontal and vertical axes are in kilometers.

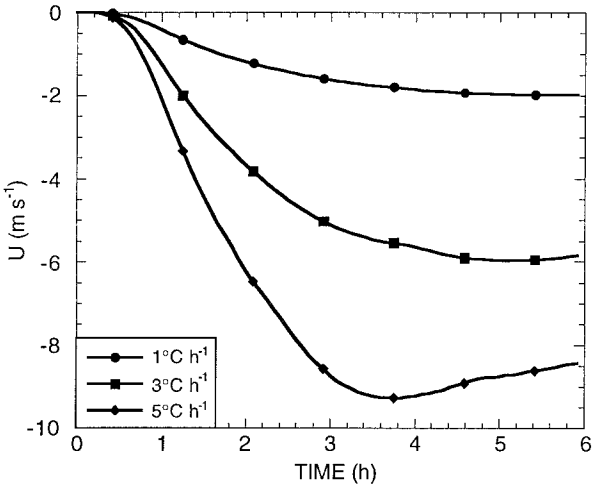

FIG. 17. Time rate of change of the divergent u component of the wind for the three heating rates (1°, 3°, and 5°C h^{-1}) for the no-jet control experiments (1a–c).

by Seman (1994), Raymond (1992), and others. The presence of this inertially unstable region can lead to the mesoscale Conv-SI described by Seman (1991).

The other two control experiments (1a, 1c) at 40° latitude use different heating rates (Table 2). Figure 17 shows the strength of the u winds as a function of time for the three heating rates for experiments 1a–c. As expected, there is a stronger response for greater heating. As a consequence of stronger outflow and horizontal advection, the location of the rotational v wind maximum and associated vorticity pattern (not shown) is displaced outward from the heating core for stronger heating rates. This important result serves to emphasize how regions with stronger heating (and stronger outflow) can exert an influence over larger distances, eventually attaining scales comparable with the Rossby radius of deformation.

Experiments 1d–f are identical to 1a–c, respectively, except for latitude (25°). Because of the lower latitude and reduced Coriolis force, adjustment to geostrophic balance is slower and divergence more persistent.

For the largest heating rate ($H_0 = 5$°C h^{-1}) and after 6 h, the divergent u wind (Table 3) is stronger (± 9.2 m s^{-1}; experiment 1f) at the lower latitude than for the equivalent high-latitude experiment (± 8.4 m s^{-1}; experiment 1c). This is an ample demonstration of how Coriolis acts to control the rate of cross-stream divergence. The rotational v wind (not shown) was also smaller by a factor of 2 for the low-latitude case. Thus, at low latitudes, geostrophic adjustment is slower and more of the wind is in the divergent component than in the rotational component for the 6-h duration of these experiments.

The results discussed here are not unexpected; that is, the development of an upper-level anticyclone, divergent flow aloft, and convergent flow in the lower and middle levels have been observed both in observational and modeling studies for many years. It is important, however, that this step be taken so that the remaining experiments have a benchmark for proper comparison. Differences between the control experiments and subsequent experiments can then be readily attributed to the presence of a jet in the latter.

TABLE 3. Comparison of maximum values (left) and at $t = 6$ h (right) of the u component of the wind (westerly, top; easterly, middle) and vertical velocity w (bottom) for each heating rate ($H_0 = 1°$, 3°, and 5°C h^{-1}) and for each jet speed ($V_0 = 0$, 10, 20, and 30 m s^{-1}). Top entries are for experiments at latitude 40°; bottom entries at latitude 25°.

Heating rate H_0	Jet strength V_0 (m s^{-1})							
	$V_0 = 0$ (exp. 1)		$V_0 = 10$ (exp. 2)		$V_0 = 20$ (exp. 3)		$V_0 = 30$ (exp. 4)	
(°C h^{-1})	Max.	$t = 6$ h	Max.	$t = 6$ h	Max.	$t = 6$ h	Max.	$t = 6$ h
$\phi = 40°$								
1 (a)	+2.00	+2.00	+2.06	+2.06	+2.11	+2.11	+2.16	+2.16
	−1.99	−1.99	−2.25	−2.25	−2.55	−2.55	−2.92	−2.92
	+0.11	+0.11	+0.12	+0.12	+0.12	+0.12	+0.14	+0.13
3 (b)	+5.98	+5.87	+6.18	+6.04	+6.29	+6.13	+6.43	+6.22
	−5.97	−5.85	−6.53	−6.48	−7.25	−7.25	−8.30	−8.30
	+0.31	+0.28	+0.33	+0.30	+0.34	+0.31	+0.36	+0.33
5 (c)	+9.31	+8.47	+9.55	+8.60	+9.65	+8.54	+9.79	+8.58
	−9.27	−8.43	−9.78	−9.23	−10.32	−10.21	−11.56	−11.56
	+0.49	+0.43	+0.51	+0.45	+0.52	+0.47	+0.54	+0.49
$\phi = 25°$								
1 (d)	+2.32	+2.32	+2.36	+2.36	+2.43	+2.43	+2.83	+2.83
	−2.31	−2.31	−2.55	−2.55	−2.73	−2.73	−3.08	−3.08
	+0.12	+0.12	+0.13	+0.13	+0.13	+0.13	+0.14	+0.14
3 (e)	+6.58	+6.56	+6.75	+6.71	+6.78	+6.71	+6.97	+6.81
	−6.56	−6.55	−7.20	−7.20	−7.80	−7.80	−9.05	−9.05
	+0.32	+0.29	+0.34	+0.31	+0.34	+0.31	+0.35	+0.33
5 (f)	+9.81	+9.24	+10.01	+9.30	+10.02	+9.32	+10.26	+9.41
	−9.78	−9.20	−10.28	−10.10	−11.00	−11.00	−12.74	−12.74
	+0.49	+0.45	+0.51	+0.46	+0.51	+0.46	+0.53	+0.48

b. Experiments 4a–f

This set of experiments has a jet imposed on the base-state winds. The jet forcing uses (3) to accelerate the v wind over a 72-h period (Fig. 18a) as discussed in section 4. The adjustment engendered by the continuous acceleration of the v winds over the 72-h period also causes a small response in the u winds (less than ± 0.25 m s^{-1}; not shown). Since this is much less than the heating-induced response in the u winds in the control experiments, we may simply use the magnitude of the u wind to compare the response to heating under various environmental conditions. Nonetheless, it is reasonable for one to ask if there is some residual ''sloshing'' remaining after the jet spinup. Integrations run for 6 h beyond the jet spinup without heating (not shown) indicate that there is a residual, but it is considerably smaller than the difference between the easterly and westerly components of the outflow when heating is present.

The jet forcing function (3) uses a value of 30 m s^{-1} for V_0,[6] but the realized value for the fully developed jet is only 18 m s^{-1} (Fig. 18a). A portion of the forcing has gone into adjustment of the mass field through geostrophic adjustment during spinup, and a small portion of it has been lost to small numerical diffusion in the model.

Figure 18b depicts the thermal field at 72 h ($t = 0$ h), illustrating this adjustment of the mass field. Figure 18c shows how the formation of the jet has created a vorticity dipole, with large positive values in the left half, and smaller positive and slightly negative values in the right half. This initial setup corresponds to a weakly inertially unstable environment.

Experiment 4b uses an H_0 in (4) of 3°C h^{-1}. The evolution of the u wind is qualitatively similar to that in the control experiments. However, after 3–4 h, the outflow at the top of the heating region has become stronger toward the west (left) into the initially inertially unstable region than toward the east (right) where the environment is inertially stable.

By $t = 6$ h, the easterly u winds are exceeding -8.3 m s^{-1}, whereas the westerly regime reaches a maximum only slightly in excess of $+6.2$ m s^{-1} (Fig. 19a). The rotational v component of the flow has also been significantly perturbed (Fig. 19b). Instead of a nearly circular jet with only slight variations in the gradient, there is now a strengthening of the gradient and speed in the region between the heating and the jet core. Starting with a vorticity couplet with values only slightly less than zero initially (see Fig. 18c), we now have a region (Fig. 19c) that is strongly negative and, consequently, inertially unstable. The modification of u, v, and ζ is a consequence of the mesoscale ascent in the heating region; tilting of quasi-horizontal vortex lines associated

[6] Here and henceforth, V_0 is used as a label for the various experiments, so that for convenience, V_0 appearing in (3) is multiplied by the 72-h spinup time to put it into units of velocity.

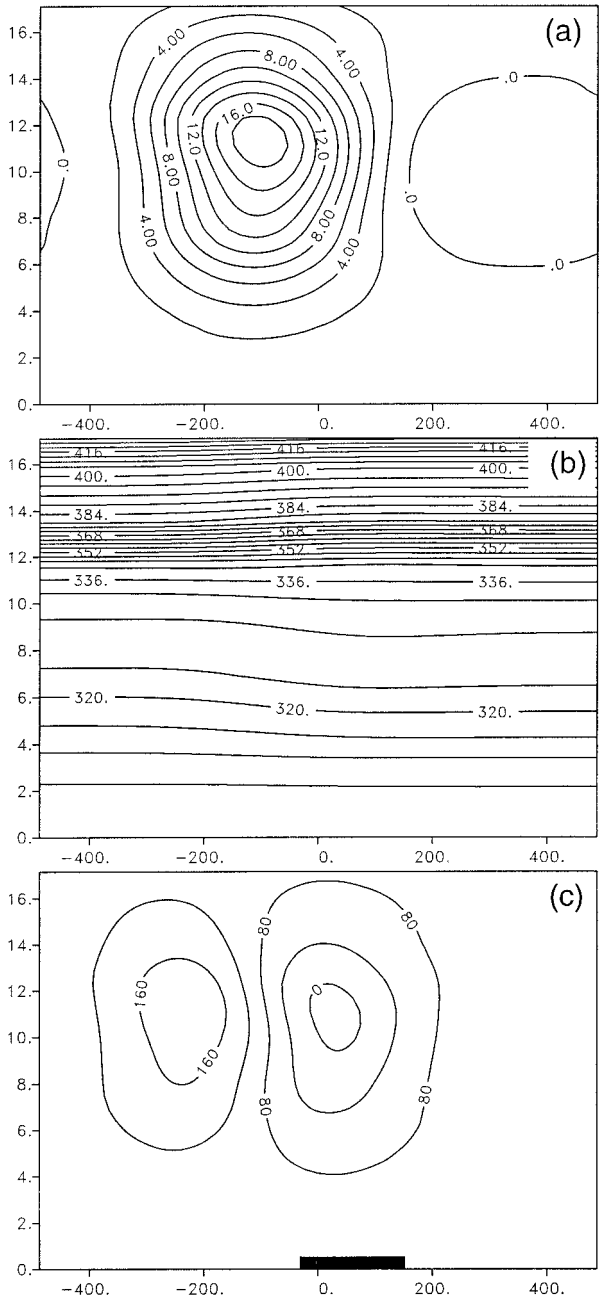

FIG. 18. Vertical cross section at $t = 0$ h for experiments 4a–c for (a) the v component of the wind (contour interval, 2 m s^{-1}), (b) the potential temperature θ (contour interval, 4 K), and (c) absolute vorticity (contour interval, 40×10^{-6} s^{-1}; negative values, dashed). The heavy bar at the bottom indicates the horizontal extent of the imposed heating. The horizontal and vertical axes are in kilometers.

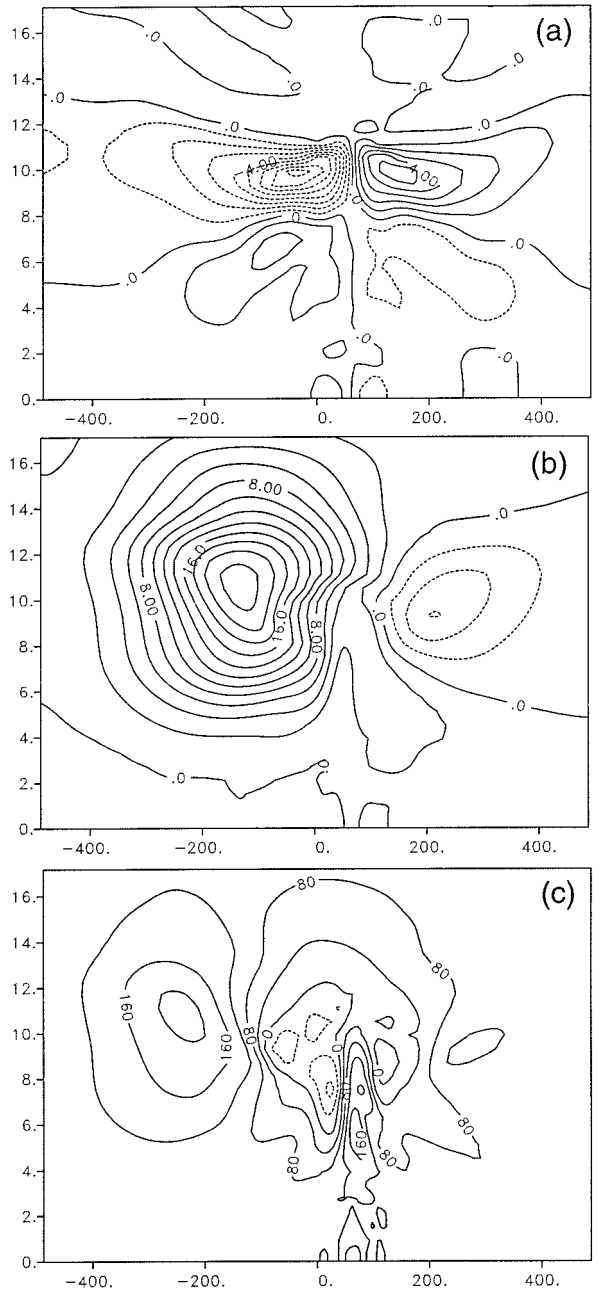

FIG. 19. Vertical cross section at $t = 6$ h for experiment 4b for (a) the u component of the wind (contour interval, 1.0 m s^{-1}), (b) the v component of the wind (contour interval, 2 m s^{-1}), and (c) absolute vorticity (contour interval, 40×10^{-6} s^{-1}; negative values, dashed). The horizontal and vertical axes are in kilometers.

with the jet accounts for the vorticity changes on either side of the mesoscale heating-induced ascent, and advection of higher vorticity from below causes the strong horizontal gradient to be displaced slightly to the left of the center of the heating region.

We now turn to another experiment using the same jet forcing and the same heating ($V_0 = 30$ m s^{-1}; $H_0 =$ 3°C h^{-1}) but with a weaker Coriolis acceleration (experiment 4e). After 72 h of acceleration ($t = 0$; not shown), the u winds are similar to those in experiment 4b. The jet has a maximum of 20 m s^{-1}, slightly greater than the equivalent experiment at a higher latitude. The vorticity couplet has a slightly weaker positive branch and the negative region has greater magnitudes than in

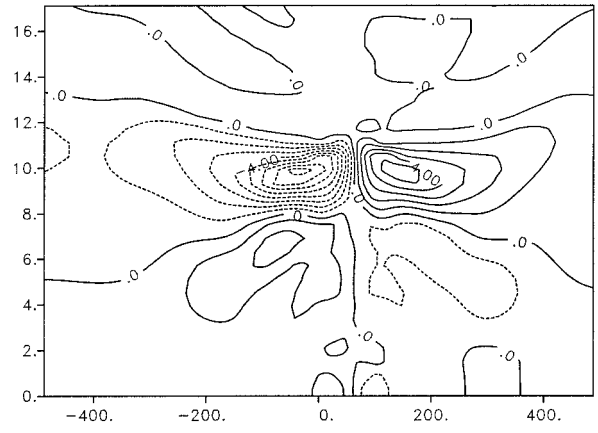

FIG. 20. Vertical cross section at $t = 6$ h of the u component of the wind (contour interval, 1.0 m s^{-1}) for experiment 4e. The horizontal and vertical axes are in kilometers.

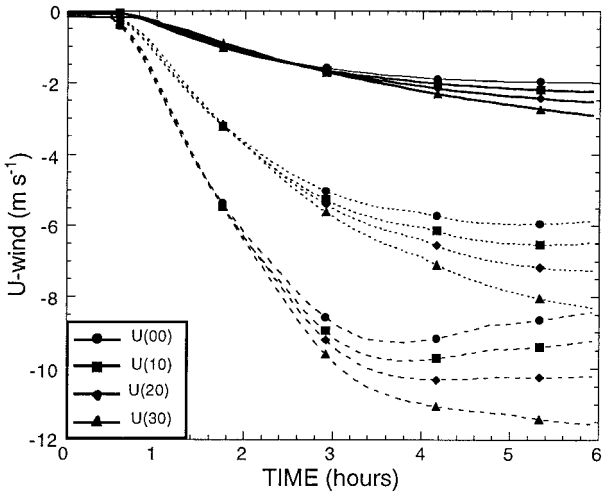

FIG. 21. Time profiles showing the rate of change of the u component of the wind for the four strengths of the jet (0, 10, 20, and 30 m s^{-1}) for heating rates of 1°C h^{-1} (solid curves), 3°C h^{-1} (dotted curves), and 5°C h^{-1} (dashed curves). The latitude is 40°.

the previous experiment, resulting in a larger region of inertial instability.

The divergent u winds develop in a manner similar to that in experiment 4b, except that the speeds are typically greater at equivalent times. This trend continues until $t = 6$ h when the easterly current has attained speeds of -9.1 m s^{-1}, whereas the westerly current is considerably weaker with speeds of only $+6.8$ m s^{-1} (Fig. 20). Compare this with the wind speeds of -8.3 m s^{-1} and $+6.2$ m s^{-1} attained in experiment 4b. As in the previous experiments, the development of the rotational component has modified the larger-scale jet so that the gradient and magnitude of winds are considerably stronger over a portion of the wind field. The vorticity has become large and negative in this region, leading to large values of inertial instability.

c. Comparison of control experiments 1a–f with experiments 4a–f

Results of experiments 4a–f are markedly different from the results of the control group. In the latter, the results of the outflow were symmetric about the axis of the maximum heating. The vorticity pattern developed as a result of the evolution of an anticyclone above the level of maximum heating. With time, the vorticity developed a symmetric pattern of inertial instability next to the region of maximum heating, with a region of moderate inertial stability laterally displaced from the unstable region.

In the presence of a horizontally sheared wind due to a jet, the evolution was different. An anticyclone developed aloft above the level of maximum heating, and this local vorticity pattern was superimposed on the larger-scale vorticity. The presence of the jet is associated with a dipole vorticity pattern having a region of moderate-to-strong absolute vorticity to the left (west) of the horizontal wind speed maximum, and a region of small positive and slightly negative values to its right (east). As the heating-induced flow modified this vorticity field, the region of inertial instability grew in magnitude and size. This increased instability permits greater cross-stream accelerations of the easterly outflow and ageostrophic horizontal advection of lower v momentum brought up from below, resulting in a strengthened gradient on the anticyclonic side of the jet. Further, the growth of the divergent easterly outflow across the jet advects the anticyclonic, rotational v wind that developed in situ to the west (left) of the heating region, resulting in a small increase of the jet strength (cf. Figs. 18a and 19b). These features all work together in a positive feedback process, continually increasing the gradient and magnitude of the jet, resulting in additional instability and causing greater accelerations of the easterly outflow. Thus, we have shown that the presence of a heat source in a region that is inertially unstable can lead to a positive feedback process, as pointed out by Eliassen (1951) and discussed earlier in section 2.

It was also shown that the response generated for a given jet and heating strength was greater at lower latitudes. This is simply the result of the fact that at the lower latitudes the geostrophic adjustment time is slower and the outflow is allowed to expand farther and at greater speeds.

d. Comparison of experiments 1–4

As shown in Table 2, many experiments were conducted using various jet speeds, heating intensities, and latitudes. Instead of discussing these individually, we present Figs. 21 and 22 and Table 3 to illustrate how the variations of the strength of the jet, heating rates, and latitude can affect the integration.

Figure 21 depicts the strength of the divergent u component of the wind for each of the three heating profiles

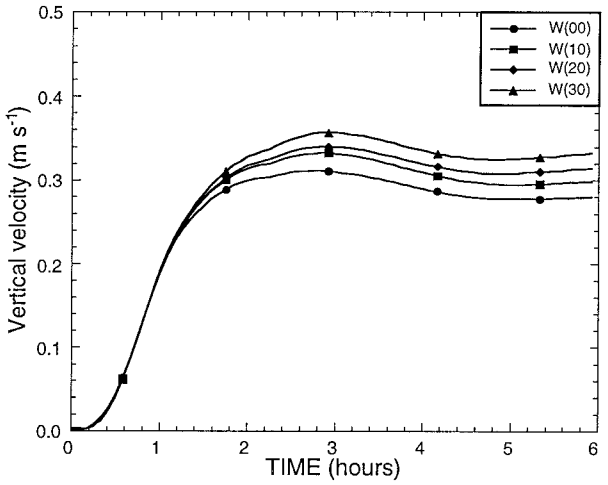

FIG. 22. Time profiles showing the rate of change of the vertical velocity strengths of the jet (0, 10, 20, and 30 m s^{-1}) for a heating rate of 3°C h^{-1}. The latitude is 40°.

(1°, 3°, and 5°C h^{-1}) at 40° latitude for each of the four jet strengths (0, 10, 20, and 30 m s^{-1}). Examination of the (four) curves within each heating rate shows that by approximately 3 h there are differences in the strength of the outflow that are jet dependent. By the end of the experiment at 6 h, the differences are greatest, although the slope of the curves suggests that rates of change are decreasing, especially for the strongest heating rate. The results for the low-latitude experiments ($\varphi = 25°$; not shown) are similar to those for the high-latitude experiments. The differences in the strength of the outflow associated with the different jet speeds take slightly longer to manifest themselves (about 3.5 h) than in the higher-latitude case. Also, the absolute strength of the outflow is increased by about 9% in the low-latitude cases compared with the high latitude; these increases are a direct consequence of the increased adjustment time at the lower latitude.

These results show that given similar heating and wind profiles, less upper-level divergence and outflow are present with increased Coriolis force. This suggests a latitudinal dependency of the inertial instability process; that is, the Coriolis force at higher latitudes may present a restoring force that cannot be overcome with the strengths of typical convective-season jet streaks. Observations have suggested that mesoscale convective systems are more likely to occur in lower and middle latitudes than in higher latitudes. Of course, the lack of high-latitude systems may simply be due to a lack of sufficient low-level moisture being advected northward to provide the fuel for the system; nonetheless, the results presented here suggest that this may be another factor that must be considered.

The speeds of the upper-level outflow winds that have a westerly component—that is, the winds diverging from the right side of the heating function (positive-valued winds in Table 3)—show little difference between the no-jet control experiments and the strong-jet experiments. This provides ample evidence that the divergent outflow has a strong, dynamic response in the region of the inertial instability and that the response of the outflow is not symmetric about the heated region.

It should be expected with increased divergence aloft, as shown by the increase in the outflow of the *u* winds, that the vertical velocity would be affected. Figure 22 shows how the vertical velocity in the core of the heated region responds to the variations in jet stream strength. All the experiments are similar during the first few hours; differences begin to appear after about 2 h, approximately the same amount of time required for the divergence profiles to show differences. The jet-experiment vertical velocities *w* exceed the no-jet control experiments by 8%–17% for the low-latitude cases (not shown), and by 13%–18% for the high-latitude cases; variations in percentage change are related to the three different heating rates. The smaller increases at the low latitude may be a consequence of the fact that the secondary circulations are already taking advantage of a weaker restoring force compared with that at the higher latitude. This result suggests that an increase in heating rates can overcome the resistance from the Coriolis force at higher latitudes. Although this result should not be surprising (intuitively it makes sense), it is an important consequence. In other words, a positive feedback process resulting in the generation and enhancement of an inertial instability can be achieved either through a decrease in the restoring force [because of preexisting weak inertial stability, reduced Coriolis accelerations, or vertical advection of low-momentum air (discussed below)], through increased heating, or through a combination of the two.

e. Sensitivity tests

Three additional experiments were run to assess how variations in ambient static stability (experiment 5) and vertical shear (experiments 6 and 7) might affect the results. The thermodynamic data used in experiments 1–4 are from an actual sounding that has been slightly smoothed for input into the model. For experiment 5, the model input thermodynamic data specified a highly idealized sounding. This particular sounding has been used by other modelers (e.g., Weisman and Klemp 1982, 1984; Rotunno et al. 1988; Skamarock et al. 1994) for simulating supercells, MCSs, bow echoes, and other convection. For purposes of discussion, the original (actual) sounding will be referred to as OKC, and the second (idealized) sounding as WK. The two soundings are similar, but the differences are important (see Fig. 15). The WK sounding has a slightly more stable lapse rate at all levels, but especially in the upper troposphere. Both soundings define the tropopause at or near 200 mb. These experiments are discussed in the following subsections.

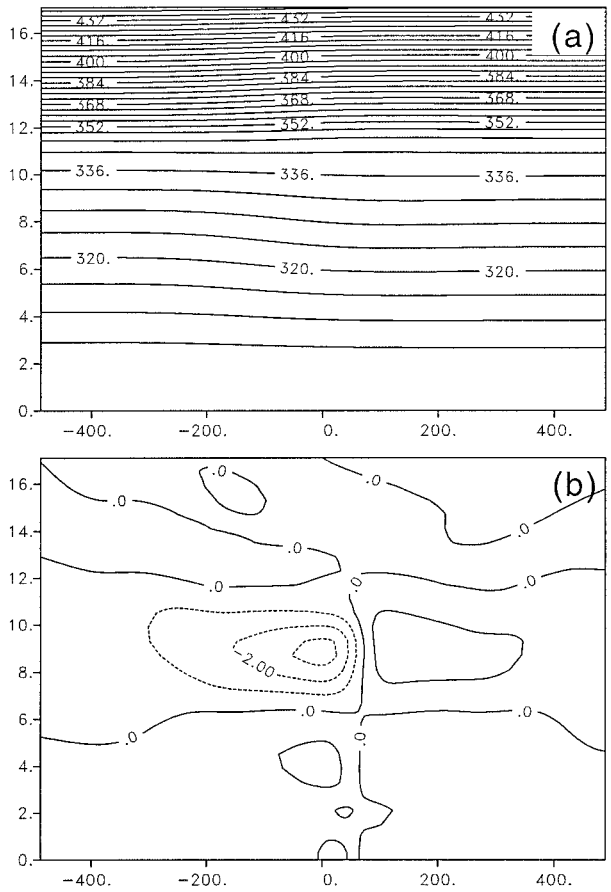

FIG. 23. Vertical cross section for experiment 5 for (a) the potential temperature θ (contour interval, 4 K) at $t = 0$ h, and (b) the u component of the wind (contour interval, 1.0 m s^{-1}) at $t = 6$ h. The horizontal and vertical axes are in kilometers.

1) STATIC STABILITY

The integrations using the WK sounding were conducted in a manner identical to the OKC experiments; however, only one jet speed, one latitude, and one heating rate were used ($V_0 = 30$ m s^{-1}, $\phi = 40°$, and $H_0 = 3°$C h^{-1}, corresponding to experiment 4b). At $t = 0$ h (i.e., after 72 h of spinup), no significant differences are noted in either the u winds or v winds. The thermal structure, on the other hand, shows the higher and more uniform static stability in experiment 5 than in experiment 4b (cf. Fig. 23a with Fig. 18b). Owing to this higher static stability, the divergent component of the horizontal flow at $t = 6$ h is weaker than in experiment 4b (cf. Fig. 23b with Fig. 19a). Not only are the u wind speeds in the WK experiment less than in the original OKC experiment, but the westerly winds expanding out on the right side of the heating profile away from the jet have also decreased from their peak value, which occurred at $t = 3$ h (not shown). This is quite different from the previous experiments (i.e., experiments 1–4) in which the winds increased or remained quasi-steady with time.

It should now be apparent that the integrations are sensitive to the *vertical* stability and as the vertical (static) stability increases, the asymmetry between the easterly and westerly outflow becomes more pronounced. Also, because of the greater vertical stability, the updrafts are weaker for a given heating rate. A possible explanation for this asymmetric behavior of the outflow is that the greater vertical stability inhibits the descending motion of the diverging air within the model domain. In the region of the jet and inertial instability, this inhibiting factor is partially offset because the thermal wind balance between the jet and the isentropes has resulted in sloped θ surfaces. These sloped surfaces provide a mechanism for adiabatic descent of the parcels along the return branch of the Conv-SI solenoid, described earlier and depicted in Fig. 2. Consequently, the presence of a region of sloped adiabatic descent permits additional air parcels to continue to diverge from the updraft and into this region to replenish the parcels evacuated through the slant downdrafts. In the stable region, on the other hand, the inhibition of downdrafts because of large static stability and the lack of tilted isentropes results in resistance to lateral spreading of outflow there and, consequently, a reduction in the divergence of parcels into this region.

2) VERTICAL SHEAR

Two additional experiments using the OKC sounding were run to evaluate the influence of vertical shear of the v component of the wind. For these experiments (6, 7), the base state included horizontally homogeneous v winds that increased in strength with height up to the level just below the tropopause, then decreased in strength above that level. This differs from all previous experiments in which the base state was at rest.[7] As in previous experiments, the v wind associated with the jet core was superimposed as a perturbation on this base state. Both experiments 6 and 7 have only one latitude and heating rate ($\phi = 40°$ and $H_0 = 3°$C h^{-1}). Experiment 6 has a single jet value ($V_0 = 30$ m s^{-1}); experiment 7 has no jet.

To evaluate the results of experiment 6, we compare it with experiment 4b, which used the same jet speed, latitude, and heating rate, but did not have a base-state vertically sheared wind. The differences between experiments 6 and 4b are most apparent at $t = 6$ h. The u wind (Fig. 24a) shows remarkable asymmetry with

[7] RAMS requires that 2D integrations use a horizontally homogeneous initialization. Because the base-state winds are independent of the base-state thermal structure, they are not in thermal wind balance, nor does the initialization have a balance of all forces. To support vertical shear like that depicted here, there should be gently sloping isentropes; however, the isentropes would remain nearly horizontal and would likely have little influence on the simulations shown here. This decoupling of the pressure and wind fields is typical of 2D model simulations.

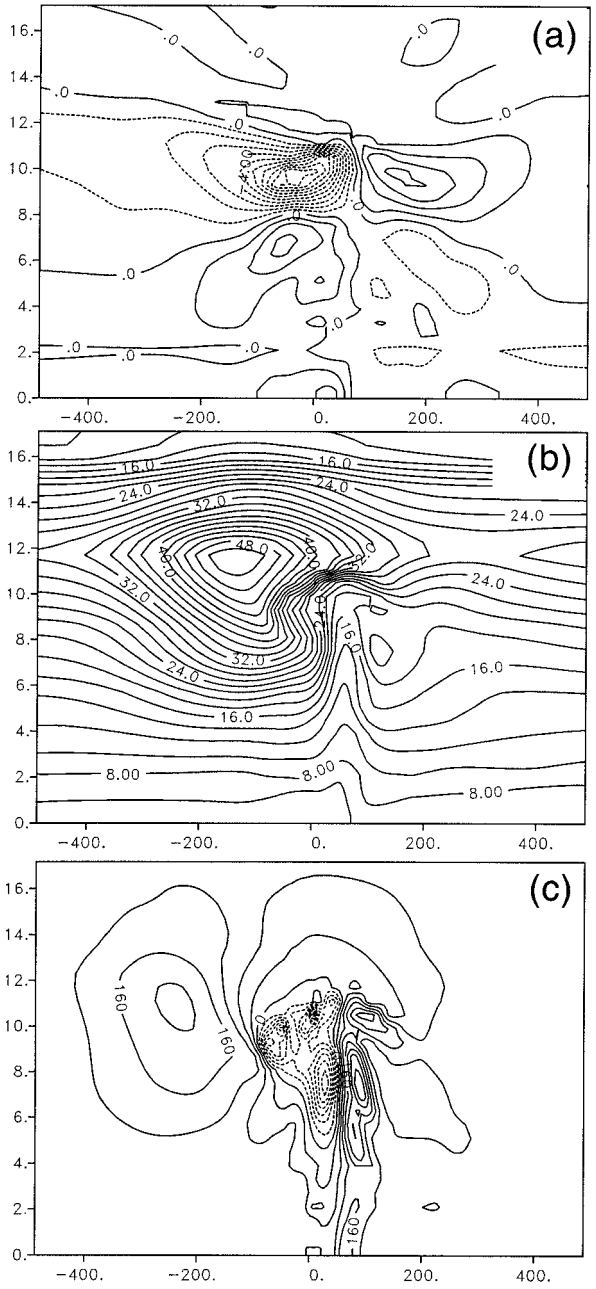

FIG. 24. Vertical cross section at $t = 6$ h for experiment 6 for (a) the u component of the wind (contour interval, 1.0 m s^{-1}), (b) the v component of the wind (contour interval, 2.0 m s^{-1}), and (c) the absolute vorticity (contour interval, 40×10^{-6} s^{-1}; negative values, dashed). The horizontal and vertical axes are in kilometers.

values of -11.0 and $+4.5$ m s^{-1}; experiment 4b had values of -8.3 and $+6.2$ m s^{-1} (Fig. 19a). What is interesting is the increase in magnitude of the easterly current and the decrease in the westerly current for experiment 6 compared with experiment 4b. Figure 24b shows the structure of the v wind after 6 h. Especially prominent is the advection of low-level, low-momentum air to upper levels. The effect of this advective process

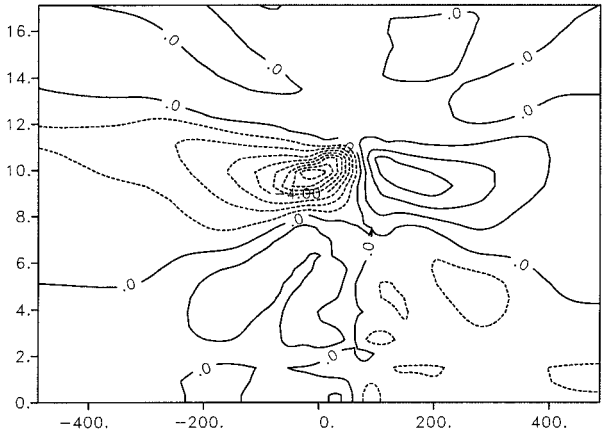

FIG. 25. Vertical cross section at $t = 6$ h for experiment 7 for the u component of the wind (contour interval, 1.0 m s^{-1}). The horizontal and vertical axes are in kilometers.

is to increase the horizontal gradient of the wind and the horizontal shear on both sides of the updraft and results in the vorticity pattern shown in Fig. 24c. The vertical advection of low-momentum air has resulted in the development of a strong inertially unstable region adjacent to a strong inertially stable region. The unstable region supports and enhances westward (leftward) cross-stream accelerations, while the strongly stable region (to the right) retards these motions. The result of these two processes is to create the highly asymmetric pattern revealed in Fig. 24a.

Finally, we present an experiment with no initial horizontal shear (i.e., no jet) but with vertical shear. The environment in this experiment is similar to that of Seman (1994), which only had vertical shear. To evaluate the results of experiment 7, we compare it with experiment 1b, which used the same latitude and heating rate but did not have a base-state vertically sheared wind.

Figure 25 shows the u winds after 6 h. There is a significant asymmetry present here that was not present in the no-shear control experiment (1b). At $t = 6$ h, the u winds are -8.9 and $+3.9$ m s^{-1}. These are quite different from the control experiment values of ± 6.0 m s^{-1}. In this experiment, as in the previous experiment 6, we have shown that the presence of a vertically sheared environment leads to asymmetries owing to the vertical advection of low-momentum air from the lower to the upper troposphere.

It is instructive to compare the divergent u winds for these last few experiments. Figure 26 is a measure of the magnitude of the outflow during the 6-h integration and is defined as $\Delta u = u_p - u_n$, where u_p (u_n) are the positive- (negative-) valued branches of the divergent outflow. The weakest Δu's are associated with experiment 1b, the no-shear control environment. The Δu's in the vertically sheared environment (experiment 7) are only slightly larger in magnitude (9% greater than the control experiment). Experiments 4b (horizontal shear) and 6 (horizontal and vertical shear) are similar to each

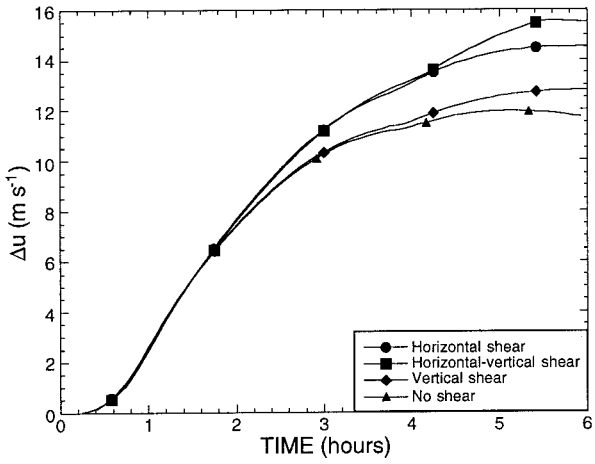

FIG. 26. Time profile showing the magnitude of the divergent outflow (m s^{-1}) defined as $\Delta u = u_p - u_n$, where u_p (u_n) are the positive- (negative-) valued branches of the outflow, for the no-shear (1b), horizontal shear (4b), horizontal and vertical shear (6), and vertical shear (7) experiments.

other and exhibit larger Δu's than the other two experiments (24% and 32% greater than the control experiment, 1b). This indicates that even though a vertically sheared environment can produce asymmetric outflows and local inertial instabilities, the magnitude of the outflow is only slightly enhanced over that of an environment with no shears. On the other hand, the presence of horizontal shears can greatly enhance the outflow, especially when vertical shears are also present. In other words, the generation of in situ inertial instabilities may locally enhance the convection by driving solenoidal circulations, but there is a greater likelihood of this occurring if there is also a preexisting meso-α-scale (or synoptic-scale) area of weak inertial instability.

6. Summary and conclusions

We have investigated the hypothesis and presented a conceptual model of how mesoscale regions of low inertial stability or weak inertial instability in the upper troposphere can contribute to the upscale growth of individual convective cells into MCSs. Features that are common to many convective system environments include the presence of a mesoscale jet streak and/or a strong subsynoptic-scale ridge. Both of these environments may contain such regions of weak isentropic inertial instability. Following are the investigations made in this study and the findings.

• The high-spatial-resolution and high-temporal-resolution rawinsonde data from the PRE-STORM field program were carefully analyzed to determine the environmental characteristics. The enhanced resolution of these data provided an unprecedented look at these features and showed that inertially unstable regions are often observed when the environment is examined with high-resolution data and may occur more frequently than commonly assumed. The standard NWS rawinsonde spacing cannot adequately sample these features, and inertially unstable regions sampled by these data will typically appear as regions of weak inertial stability.

• The high-frequency rawinsonde data were also used to examine rapid mesoscale changes due to convection. Temporal changes were computed for temperature, pressure, moisture, and winds using soundings taken 3 h apart. They revealed that strong divergence and cross-stream accelerations occurred at upper-tropospheric levels where inertial instabilities were present. These accelerations were not uniform over the domain but were focused in the regions of the instability.

• The analysis of the case studies was complemented using the Regional Atmospheric Modeling System (RAMS) to simulate inertially unstable and weakly stable environments. The first set of integrations was designed as a control experiment with no jet imposed. The results of the control experiments showed that an upper-level anticyclone develops above the convection and can generate regions of in situ inertial instability. The outflow at the top of the updraft is symmetric and divergent. The strength of the outflow is determined primarily by the intensity of the heating rate and secondarily by the resistance imposed by the Coriolis parameter.

• All the jet and heating experiments were run for two latitudes to provide understanding of the full implications of the importance of the Coriolis parameter. The results of these experiments indicate that the increase of the Coriolis force at higher latitude results in greater inertial stability for a given jet strength. This suggests that there may be a latitudinal dependency to this process; that is, the Coriolis force at higher latitudes may present a restoring force that cannot be overcome with the strength of typical convective-season jet streaks.

• For each latitude and heating rate, three jet speeds were tested. The results of these experiments showed that the stronger jets generated a greater degree of asymmetry of the outflow, indicating that the divergent, cross-stream outflow increases with decreasing inertial stability.

• An additional experiment was conducted to test the sensitivity of the integrations to the degree of static stability. The original data used to initialize RAMS were from a sounding taken prior to the development of an MCC. One of the characteristics of this sounding was the low static stability in the upper troposphere. The comparison experiments used a sounding with a more stable upper troposphere. The results indicated substantial control of the degree of asymmetry and the strength of the divergent, cross-stream outflow by the static stability.

The coexistence of convective and symmetric (or isentropic inertial) instability has been termed both ''convective-symmetric instability (Conv-SI)'' (Emanuel 1980; Seman 1991) and ''nonhydrostatic, nonlinear conditional symmetric instability'' (Seman 1994), and rep-

resents unbalanced dynamics associated with convective momentum transport and Coriolis accelerations. Seman noted that the instability starts with momentum transport in the deep convection, which creates negative isentropic absolute vorticity and the potential for symmetric instability in the upper troposphere. Coriolis accelerations allow the symmetric instability to be realized. The release of the symmetric instability creates a mesoscale outflow jet that ventilates the upper levels of the systems and assists in the development of more convection. This mesoscale jet generates in situ inertial instability that can feed back into any preexisting mesoscale instability. A positive feedback mechanism exists on mesoscale timescales because the deep convection transports more low-level momentum to the upper levels, replenishing the supply of symmetrically unstable flow aloft.

As shown in the results presented here, the presence of weak inertial instability prior to the convection greatly enhances the likelihood of this feedback process occurring. Thus, if the mesoscale environment is in a state of inertial stability, only small perturbation of this environment by convection may be required to render it inertially unstable. If the environment is already inertially unstable, the Conv-SI feedback process will occur quickly. Conversely, in an environment that is inertially very stable, the feedback process may never develop.

7. Future research

Future work should take both observational and modeling approaches to further investigate this hypothesis.

Observational investigations could focus on regions having a relatively homogeneous environment in the lower troposphere in which convection may form in multiple locations during the afternoon and early evening. An important question to answer is, do convective clusters that are located near or within regions of upper-tropospheric inertial instability continue to grow upscale during the evening/night while the other convective clusters usually dissipate with the loss of solar heating of the ground and the development of a low-level nocturnal inversion? To answer this question, it is suggested that the U.S. Weather Research Program have a high concentration of rawinsonde launch sites and wind profiler Doppler radars in the field to provide the necessary scale of coverage and resolution required to sample the preconvective environment that may contain these mesoscale instabilities.

There are two obvious extensions to the modeling component of this work. Future 3D experiments could be constructed so that they look at more complex situations such as the strongly curved, anticyclonic flow in a subsynoptic-scale ridge. Further, the work reported here demonstrates, in the context of imposed heating, the importance of preconvective inertial stability on development of an enhanced solenoidal circulation in response to convection. Thus we have established a rational basis for more complex experiments in which the moist convection is simulated explicitly and is allowed to produce and to fully interact with the solenoidal circulation. Such experiments will allow more complete studies of how certain configurations of preconvective inertial stability may lead to upscale growth of mesoscale convective systems.

Acknowledgments. A portion of the data used in this study was made available by the invaluable contributions of many scientists during the PRE-STORM field program. In particular, I would like to thank Mr. John Cunning (NOAA/FSL), PRE-STORM Project Director. I would also like to thank Dr. Stanley Benjamin and Ms. Tracy Lorraine Smith (NOAA/FSL) for providing the MAPS mesoscale analysis products and software. Mr. John Augustine (NOAA/ARL) graciously provided the results of his compositing study of MCCs. Dr. Rolf Hertenstein (CSU) provided the original code for the heating functions used in this study. This research was supported in part under National Science Foundation Grant ATM-9118963.

REFERENCES

Augustine, J. A., and F. Caracena, 1994: Lower-tropospheric precursors to nocturnal MCS development over the central United States. *Wea. Forecasting,* **9,** 116–135.

Barnes, S. L., 1985: Omega diagnostics as a supplement to LFM/MOS guidance in weakly forced convective situations. *Mon. Wea. Rev.,* **113,** 2122–2141.

Bartels, D. L., and R. A. Maddox, 1991: Midlevel cyclonic vortices generated by mesoscale convective complexes. *Mon. Wea. Rev.,* **119,** 104–118.

Benjamin, S. G., K. A. Brewster, R. L. Brummer, B. F. Jewett, T. W. Schlatter, T. L. Smith, and P. A. Stamus, 1991: An isentropic three-hourly data assimilation system using ACARS aircraft observations. *Mon. Wea. Rev.,* **119,** 888–906.

——, J. M. Brown, K. J. Brundage, D. Devenyi, B. E. Schwartz, T. G. Smirnova, T. L. Smith, and F.-J. Wang, 1996: The 40-km 40-level version of MAPS/RUC. Preprints, *11th Conf. on Numerical Weather Prediction,* Norfolk, VA, Amer. Meteor. Soc., 161–163.

Bennetts, D. A., and B. J. Hoskins, 1979: Conditional symmetric instability—A possible explanation for frontal rainbands. *Quart. J. Roy. Meteor. Soc.,* **105,** 945–962.

Bjerknes, J., 1951: Extratropical cyclones. *Compendium of Meteorology,* T. F. Malone, Ed., Amer. Meteor. Soc., 577–598.

Blanchard, D. O., 1990: Mesoscale convective patterns of the southern High Plains. *Bull. Amer. Meteor. Soc.,* **71,** 994–1005.

——, 1995: Jet-induced inertial instabilities and the growth of mesoscale convective systems. Dept. of Atmospheric Science Paper 571, Colorado State University, 191 pp. [Available from Dept. of Atmospheric Science, Colorado State University, Fort Collins, CO 80523.]

Bretherton, C. S., and P. K. Smolarkiewicz, 1989: Gravity waves, compensating subsidence and detrainment around cumulus clouds. *J. Atmos. Sci.,* **46,** 740–759.

Caracena, F., 1987: Analytic approximation of discrete field samples with weighted sums and gridless computation of derivatives. *J. Atmos. Sci.,* **44,** 3753–3768.

Charney, J. G., and A. Eliassen, 1964: On the growth of the hurricane depression. *J. Atmos. Sci.,* **21,** 68–75.

Churchill, D. D., and R. A. Houze Jr., 1984: Development and structure of winter monsoon cloud clusters on 10 December 1978. *J. Atmos. Sci.,* **41,** 933–960.

Cotton, W. R., R. L. George, P. J. Wetzel, and R. L. McAnelly, 1983: A long-lived mesoscale convective complex. Part I: The mountain-generated components. *Mon. Wea. Rev.,* **111,** 1893–1918.

——, M. Lin, R. L. McAnelly, and C. J. Tremback, 1989: A composite model of mesoscale convective complexes. *Mon. Wea. Rev.,* **117,** 765–783.

Cunning, J. B., 1986: The Oklahoma–Kansas preliminary regional experiment for STORM-Central. *Bull. Amer. Meteor. Soc.,* **67,** 1478–1486.

Eliassen, A., 1951: Slow thermally or frictionally controlled meridional circulation in a circular vortex. *Astrophys. Norv.,* **5,** 19–60.

Emanuel, K. A., 1979: Inertial instability and mesoscale convective systems. Part I: Linear theory of inertial instability in rotating viscous fluids. *J. Atmos. Sci.,* **36,** 2425–2449.

——, 1980: Forced and free mesoscale motions in the atmosphere. *Collection of Lecture Notes on Dynamics of Mesometeorological Disturbances, CIMMS Symposium,* Norman, OK, University of Oklahoma/NOAA, 189–259.

——, 1982: Inertial instability and mesoscale convective systems. Part II: Symmetric CISK in a baroclinic flow. *J. Atmos. Sci.,* **39,** 1080–1097.

——, 1983: The Lagrangian parcel dynamics of moist symmetric instability. *J. Atmos. Sci.,* **40,** 2368–2376.

Fovell, R. G., 1991: Influence of the Coriolis force on a two-dimensional model storm. *Mon. Wea. Rev.,* **119,** 603–630.

Hertenstein, R. F. A., and W. H. Schubert, 1991: Potential vorticity anomalies associated with squall lines. *Mon. Wea. Rev.,* **119,** 1663–1672.

Hoskins, B. J., and M. A. Pedder, 1980: The diagnosis of middle latitude synoptic development. *Quart. J. Roy. Meteor. Soc.,* **106,** 707–719.

——, I. Draghici, and H. Davies, 1978: A new look at the ω-equation. *Quart. J. Roy. Meteor. Soc.,* **104,** 31–38.

Jascourt, S. D., S. S. Lindstrom, C. J. Seman, and D. D. Houghton, 1988: An observation of banded convective development in the presence of weak symmetric stability. *Mon. Wea. Rev.,* **116,** 175–191.

Johnson, R. H., and P. J. Hamilton, 1988: The relationship of surface pressure features to the precipitation and airflow structures of an intense midlatitude squall line. *Mon. Wea. Rev.,* **116,** 1444–1472.

Kane, R. J., C. R. Chelius, and J. M. Fritsch, 1987: Precipitation characteristics of mesoscale convective weather systems. *J. Climate Appl. Meteor.,* **26,** 1345–1357.

Klemp, J. B., and R. B. Wilhelmson, 1978: The simulation of three-dimensional convective storm dynamics. *J. Atmos. Sci.,* **35,** 1070–1096.

Leary, C. A., 1984: Precipitation structure of the cloud clusters in a tropical easterly wave. *Mon. Wea. Rev.,* **112,** 313–325.

Maddox, R. A., 1980: Mesoscale convective complexes. *Bull. Amer. Meteor. Soc.,* **61,** 1374–1387.

——, 1983: Large-scale meteorological conditions associated with midlatitude convective complexes. *Mon. Wea. Rev.,* **111,** 1475–1493.

Mapes, B. E., 1993: Gregarious tropical convection. *J. Atmos. Sci.,* **50,** 2026–2037.

McAnelly, R. L., and W. R. Cotton, 1986: Meso-β-scale characteristics of an episode of meso-α-scale convective complexes. *Mon. Wea. Rev.,* **114,** 1740–1770.

——, and ——, 1989: The precipitation life cycle of mesoscale convective complexes over the central United States. *Mon. Wea. Rev.,* **117,** 784–808.

——, and ——, 1992: Early growth of mesoscale convective complexes: A meso-β-scale cycle of convective precipitation? *Mon. Wea. Rev.,* **120,** 1851–1877.

Menard, R. D., and J. M. Fritsch, 1989: A mesoscale convective complex-generated inertially stable warm core vortex. *Mon. Wea. Rev.,* **117,** 1237–1261.

Nachamkin, J. E., R. L. McAnelly, and W. R. Cotton, 1994: An observational analysis of a developing mesoscale convective complex. *Mon. Wea. Rev.,* **122,** 1168–1188.

Nicholls, M. E., R. A. Pielke, and W. R. Cotton, 1991: Thermally forced gravity waves in an atmosphere at rest. *J. Atmos. Sci.,* **48,** 1869–1884.

Ooyama, K., 1964: A dynamical model for the study of tropical cyclone development. *Geofis. Intl.,* **4,** 187–198.

——, 1969: Numerical simulation of the life cycle of tropical cyclones. *J. Atmos. Sci.,* **26,** 3–40.

Pielke, R. A., and Coauthors, 1992: A comprehensive meteorological modeling system—RAMS. *Meteor. Atmos. Phys.,* **49,** 69–91.

Raymond, D. J., 1992: On the formation of jets and vortices in mesoscale convective systems. Preprints, *Fifth Conf. on Mesoscale Processes,* Atlanta, GA, Amer. Meteor. Soc., 333–336.

——, and H. Jiang, 1990: A theory for long-lived mesoscale convective systems. *J. Atmos. Sci.,* **47,** 3067–3077.

Rotunno, R., J. B. Klemp, and M. L. Weisman, 1988: A theory for strong long-lived squall lines. *J. Atmos. Sci.,* **45,** 463–485.

Schaefer, J. T., 1986: The dryline. *Mesoscale Meteorology and Forecasting,* P. Ray, Ed., Amer. Meteor. Soc., 549–572.

Schubert, W. H., and J. J. Hack, 1982: Inertial stability and tropical cyclone development. *J. Atmos. Sci.,* **39,** 1687–1697.

——, ——, P. L. Silva Dias, and S. R. Fulton, 1980: Geostrophic adjustment in an axisymmetric vortex. *J. Atmos. Sci.,* **37,** 1464–1484.

Seman, C. J., 1990: Numerical simulation of deep moist convection in a baroclinic atmosphere. Preprints, *Fourth Conf. on Mesoscale Processes,* Boulder, CO, Amer. Meteor. Soc., 104–105.

——, 1991: Numerical study of nonlinear convective-symmetric instability in a rotating baroclinic atmosphere. Ph.D. dissertation, University of Wisconsin—Madison, 185 pp. [Available from Dept. of Atmospheric and Oceanic Sciences, University of Wisconsin—Madison, Madison, WI 53706.]

——, 1994: A numerical study of nonlinear nonhydrostatic conditional symmetric instability in a convectively unstable atmosphere. *J. Atmos. Sci.,* **51,** 1352–1371.

Skamarock, W., M. L. Weisman, and J. B. Klemp, 1994: Three-dimensional evolution of simulated long-lived squall lines. *J. Atmos. Sci.,* **51,** 2563–2584.

Stevens, D. E., and P. E. Cielsielski, 1986: Inertial instability of horizontally sheared flow away from the equator. *J. Atmos. Sci.,* **43,** 2845–2856.

Thorpe, A. J., M. J. Miller, and M. W. Moncrieff, 1982: Two-dimensional convection in nonconstant shear: A model of midlatitude squall lines. *Quart. J. Roy. Meteor. Soc.,* **108,** 739–762.

Tripoli, G. J., and W. R. Cotton, 1989a: Numerical study of an observed orogenic mesoscale convective system. Part 1: Simulated genesis and comparison with observations. *Mon. Wea. Rev.,* **117,** 273–304.

——, and ——, 1989b: Numerical study of an observed orogenic mesoscale convective system. Part 2: Analysis of governing dynamics. *Mon. Wea. Rev.,* **117,** 305–328.

Weisman, M. L., and J. B. Klemp, 1982: The dependence of numerically simulated convective storms on vertical shear and buoyancy. *Mon. Wea. Rev.,* **110,** 504–520.

——, and ——, 1984: The structure and classification of numerically simulated convective storms in directionally varying wind shears. *Mon. Wea. Rev.,* **112,** 2479–2498.

Wetzel, P. J., W. R. Cotton, and R. L. McAnelly, 1983: A long-lived mesoscale convective complex. Part II: Evolution and structure of the mature complex. *Mon. Wea. Rev.,* **111,** 1919–1937.

Xu, Q., 1986: Conditional symmetric instability and mesoscale rainbands. *Quart. J. Roy. Meteor. Soc.,* **112,** 315–334.